The evolution of REE mineralisation within the Ditrău Alkaline Complex, Romania: interplay of magmatic and hydrothermal processes

V. C. Honour[1,2]; K. M. Goodenough[3]; R. A. Shaw[4]; I. G. Radulescu[5]; P.Hirtopanu[6]

[1] Department of Earth Sciences, University of Cambridge, Cambridge, CB2 3EQ, UK; vch28@cam.ac.uk
[2] Camborne School of Mines, University of Exeter, Penryn, Cornwall, TR10 9FE, UK
[3] British Geological Survey, the Lyell Centre, Research Avenue South, Edinburgh EH14 4AP, UK
[4] British Geological Survey, Environmental Science Centre, Keyworth, Nottingham NG12 5GG, UK
[5] 012424 Bucharest, Romania
[6] Department of Mineralogy, University of Bucharest, Romania

ABSTRACT

The Ditrău Igneous Complex (NE Romania) is a tilted Mesozoic layered alkaline intrusion (~19 km diameter), with enrichments in rare earth elements (REE), niobium, tantalum and molybdenum. It has the potential to contribute to a secure and sustainable European REE mining industry, ensuring supply security for these critical metals. The complex comprises layered ultramafic rocks, alkali gabbros, diorites, syenites, nepheline syenites and alkali granites. These units have been significantly modified by sub-solidus interaction with late-stage magmatic fluids and are cut by secondary mafic dykes, which formed after the intrusion solidified. The complex was subsequently cut by REE-mineralised carbonate-rich veins. Geochemical and petrological data, including apatite mineral chemistry, from the alkaline igneous rocks, dykes and veins within the Ditrău Complex, have been used to assess the interplay of magmatic processes with late-stage magmatic and hydrothermal fluids, and the effects of these processes on element remobilisation and concentration of critical metals. Only limited critical metal enrichment was achieved by magmatic processes; the REE were preferentially incorporated into titanite and apatite in ultramafic cumulates during primary crystallisation, and were not enriched in evolved magmas. A hydrothermal system developed within the Ditrău Complex magma chamber at the later stages of magmatic crystallisation, causing localised alteration of nepheline syenites by a sodium-rich fluid. Later mafic dykes subsequently acted as conduits for late stage, buoyant potassic fluids, which leached REE and HFSE from the surrounding syenitic rocks. These fluids percolated up and accumulated in the roof zone, causing the breakdown of nepheline to K-rich pseudomorphs and the precipitation of hydrothermal minerals such as zircon and pyrochlore within veins. REE mineralisation within the Ditrău Complex is hosted in the latest hydrothermal phase, mineralised carbonate-rich veins which cross-cut the complex. Monazite is the main REE-bearing phase which crystallised from a late REE- and carbonate-rich fluid with pH controlled REE deposition.

KEYWORDS

Ditrău Complex, Romania; Alkaline Layered Intrusion; late-stage magmatic fluids; REE mineralisation

INTRODUCTION

Rare earth elements (REE) and other 'critical metals' are vital to many of today's technologies, crucial to providing competitive, yet sustainable economic growth (Graedel et al., 2014). Within the European Union, REE have been recognised as having clear supply risks and being of significant economic importance, pushing them onto the critical metals agenda and ensuring a focus from the European Commission (EC) (European Commission, 2017). Recycling of REE is minimal, despite ongoing research (Binnemans et al., 2013; Reck and Graedel, 2012; Schulze and Buchert, 2016; Tanaka et al., 2012), and REE substitutes are generally less effective (Stegen, 2015). Consequently, future supply will require primary extraction (U.S. Geological Survey, 2015). In 2017, global supply of REE came from a very limited number of countries, with China supplying 95% of HREE and 95% of LREE (European Commission, 2017). Restriction to the global supply of rare earths would have negative impacts, not only technological but also for national security (Humphreys, 2014). Europe's rare earth resources are under-studied with no current production from primary resources. Yet domestic REE deposits have the potential to supply all of Europe's demand for the foreseeable future (Goodenough et al., 2016). The European Commission-funded EURARE project (www.eurare.org) aims to establish the basis for sustainable REE mining and production within Europe, thus increasing supply security for Europe-based manufacturers and consumers (Balomenos et al., 2017).

Currently the most studied REE deposits in Europe are associated with either carbonatites (e.g. Fen in Norway) or with highly peralkaline igneous rocks (e.g. Norra Kärr in Sweden and Kvanefjeld and Kringlerne in the Ilímaussaq Complex of west Greenland; Upton et al., 2003; Holtstam et al., 2014; Goodenough et al., 2016). However, REE mineralisation also exists in association with hydrothermally altered alkaline igneous rocks. In this paper we describe one such intrusion with late-stage hydrothermal REE mineralisation: the Ditrău Complex in eastern Transylvania, Romania (Fig. 1).

The Ditrău Complex is a Triassic alkaline layered intrusion (Dallmeyer et al., 1997; Fall et al., 2007; Morogan et al., 2000; Pál-Molnár et al., 2015; Pană et al., 2000) with REE, niobium (Nb) and molybdenum (Mo) mineralisation (Hirtopanu et al., 2013a, 2013b, 2010). The intrusion has exposures through the entire range of compositions formed by cumulate processes (e.g. Jakab, 1998; Morogan et al., 2000). The intrusion is cut by multiple dykes of mafic and lamprophyric lithologies (Batki et al., 2014) and carbonate veins, 1–2 m wide, which host REE mineralisation.

This paper characterises the origin of the REE mineralisation and its association with hydrothermal fluids within the Ditrău Complex. New geochemical and petrological data for key lithologies and mineralised material are correlated with field relationships to provide an integrated overview of the evolution and genesis of mineralisation, in the context of the magmatic and hydrothermal system.

GEOLOGICAL BACKGROUND: PREVIOUS WORK

The Ditrău Complex in north-east Romania was formed in the mid-Triassic, during extensional activity associated with continental rifting during Tethyan evolution (Pál-Molnár and Arva-Sos, 1995; Pană et al., 2000; Stampfli, 2000). Unlike the voluminous Central Atlantic Magmatic Province generated by rifting of the Atlantic during the Jurassic – Triassic transition (Blackburn et al., 2013), the Alpine Tethyan rifting generated minimal magmatic activity (Stampfli, 2000), so the Ditrău Complex is not part of a recognised alkaline province. The Ditrău Complex is exposed over an area of 19 by 14 km (Pál-Molnár et al., 2015) and intrudes Variscan-metamorphosed Precambrian and Cambrian crystalline basement rocks of the Bucovinian nappe within the Eastern Carpathians (Balintoni and Balica, 2013; Hoeck et al., 2009), with a 1–3 km contact aureole (Anastasiu and Constantinescu, 1978; Streckeisen and Hunziker, 1974).

In the Middle Cretaceous to Tertiary the Ditrău region was deformed by Alpine tectonic events, which formed a nappe system (Dewey et al., 1973; Krautner and Bindea, 1998; Schmid et al., 2008). The complex is now partially obscured by Pliocene-Pleistocene sediments and lacustrine deposits of the Gheorgheni and Jolotca

Basins (Codarcea et al., 1957; Krautner and Bindea, 1998) and superimposed Cenozoic magmatism of the Calimani-Gurghiu-Harghita volcanic chain (Rădulescu et al., 1973; Szakacs et al., 1997).

The majority of past study on the Ditrău Complex has focused on the igneous geology (e.g. Batki, 2009; Batki et al., 2014; Fall et al., 2007; Morogan et al., 2000; Pál-Molnár, 2010; Pál-Molnár et al., 2015) and the mineralogy of the REE-carbonate veins, (Hirtopanu et al., 2015, 2013a, 2013b, 2010). The complex has previously been described as a ring structure with successively younger intrusions becoming more felsic from west to east: ultramafics, alkali gabbros and diorites out crop in the north-west whilst syenites, nepheline syenites and alkali granites lie to the south-east (Morogan et al., (2000). Dyke intrusions have previously been considered as the culmination of the magmatic activity (Batki, 2009; Batki et al., 2014).

Key geographical areas of the Ditrău Complex are delineated by Morogan et al., (2000): the northern area around the village of Jolotca (the Jolotca region); the main area, lying to the east of the village of Ditrău (the Ditrău region); and the southern region of Lăzarea. Jolotca and Ditrău are separated by a zone of faulting (Fig 1). The area west of Ditrău is very poorly exposed.

The Jolotca area is characterised by outcrops of mafic to ultramafic igneous rocks, including alkali gabbro and alkali diorite (Morogan et al., 2000). These rocks are inferred, on the basis of gravity and magnetic surveys, to extend laterally eastward beneath the complex (Jakab, 1998). In the centre of the complex there is a hybrid zone of magma mingling and igneous brecciation that includes gabbroic, dioritic and syenitic lithologies; this combination is referred to by Streckeisen (1960) as the 'Ditró essexites' (Table 1). The transition zone from mafic to felsic lithologies occurs over c. 2 km.

The east of the complex is dominated by felsic rocks (syenites, nepheline syenites and alkali granites) which show varying degrees of alteration (Jakab, 1998; Morogan et al., 2000). Previously the undersaturated syenites of the complex have been divided into 'White Syenite' and 'Red Syenite' (Jakab, 1998). The 'Red Syenite' forms patchy bodies within the 'White Syenite'. Morogan et al. (2000) and Fall et al. (2007) refer to the 'White Syenite' as nepheline syenite because it contains fresh nepheline, which is partially replaced by cancrinite. Jakab's (1998) 'Red Syenite' contains pseudomorphs after nepheline, composed of micaceous aggregates that are indicative of nepheline alteration and haematisation (Morogan et al., 2000; Fall et al., 2007). Jakab (1998) suggests that 'Red Syenite' is hydrothermally altered to 'White Syenite' based on relict structures and the smaller volume of 'Red Syenite' observed in drill core. However, Morogan et al. (2000) consider that the nepheline syenite has been hydrothermally altered to 'Red syenite'. The 'Red Syenite' is enriched in HFSE-bearing minerals (Jakab, 1998). In this paper, a revised terminology is proposed, as described below and shown in Fig. 1.

Since the discovery of the Ditrău Complex in 1859 (Herbich, 1859), numerous genetic models have been proposed, ranging from metasomatic to magmatic in origin, and single to multiple magma emplacement events. The models include magmatic differentiation and wall-rock assimilation (Ianovici, 1938); metasomatism by a Na-rich fluid permeating the country rock (Codarcea et al., 1957); magmatic differentiation of an alkali parent magma (Streckeisen, 1960); partial-melting of silica-poor crustal rocks producing a basic magma and a sialic alkaline magma (Anastasiu and Constantinescu, 1982); and a two stage emplacement process (Pál-Molnár and Arva-Sos, 1995). This last model was superseded by Krautner and Bindea's (1998) four stage model, which compiled all isotope dates on the complex to suggest that emplacement of the Ditrău intrusion spanned a 70 Myr interval across the Triassic and Jurassic. These dates fitted with the intrusion's overall history suggested by Streckeisen and Hunziker (1974). The stages described by Krautner and Bindea (1998) are: (1) c. 230 Ma, mafic and ultramafic intrusions in the Jolotca region, dated by four K-Ar analyses and two ^{40}Ar-^{39}Ar plateau ages of 231.5 ± 0.1 Ma and 227.1 ± 0.1 Ma on hornblende (Dallmeyer et al., 1997; Streckeisen and Hunziker, 1974); (2) c. 215 Ma, gabbros, diorites, monzodiorites, monzonites, syenites and quartz syenites (Krautner and Bindea, 1998); (3) c. 165-160 Ma, intrusion of nepheline syenites and formation of the 'Ditró essexites' (of Streckeisen (1960)) by hybridisation and metasomatism, followed by a series of dykes. These lithologies were

dated by K-Ar on biotite in nepheline syenite (Streckeisen and Hunziker, 1974); (4) c. 115 Ma, final hydrothermal activity associated with nappe transport due to tectonic uplift.

These past models were based on isotope ages from the $^{40}Ar/^{39}Ar$, K-Ar and Rb/Sr systems, with the ages given direct geochronological legitimacy despite the limited precision of some of the analyses (Dallmeyer et al., 1997; Pál-Molnár and Arva-Sos, 1995; Popescu, 1985; Streckeisen and Hunziker, 1974; Zincenco, 1996). The inconsistencies, spread of data and potential for disrupted Ar degassing due to Alpine tectonics, make the models based on these ages "highly suspect" (Pană et al., 2000). Most recently, Pană et al. (2000) use U-Pb zircon ages to date a sample of syenite from near Jolotca village at 229.6 +1.7/-1.2 Ma. The ^{40}Ar-^{39}Ar dates produced by Dallmeyer et al. (1997) are within error of these U-Pb zircon ages, indicating contemporaneous emplacement of syenite and gabbroic magmas, with a relatively short magmatic evolution of the Ditrău Complex.

The igneous rocks of the Jolotca area are cut by later veins hosting REE mineralisation, generally up to 1 m wide, trending E-W and dipping 60°N (G. Jakab & M. D. Cernaianu, 2015, pers. comm.). The mineralogy comprises LREE-phosphates, LREE-silicates and LREE-carbonates, with pyrite, molybdenite, Ta and Nb-bearing phases (such as ilmenorutile), all hosted in a carbonate gangue (Hirtopanu et al., 2013a, 2010; Săbău, 2009). In the south-east, 2.5 km outside the Ditrău Complex lies another area of vein-hosted mineralisation, named Belcina. Mineralisation at Belcina is analogous to the mineralised veins at Jolotca. The Belcina veins comprise Y-phosphates, Th-silicates, zircon, minor sulfides, and Nb- and Ta-bearing phases in a carbonate gangue (Hirtopanu et al., 2013a, 2013b). Previous testwork on processing the ore from these veins cutting the Ditrău Complex has demonstrated the potential of producing mineral concentrates with high REE grades (Zlagnean et al., 2000).

The Ditrău Complex was explored for economic mineralisation during government-led exploration in the 20th century, with a focus on the cross-cutting mineralised veins. There are multiple historic adits and galleries (with associated waste dumps) in the Jolotca region, but none are currently accessible. Five deep (c. 1400 m) cores were drilled during government-led exploration. The majority of core has been lost or remains under state ownership with restricted access. However, there is a limited selection at the geological museum in Gheorgheni, Romania. To date, study of the mineralisation has not included any holistic model for the Ditrău Complex.

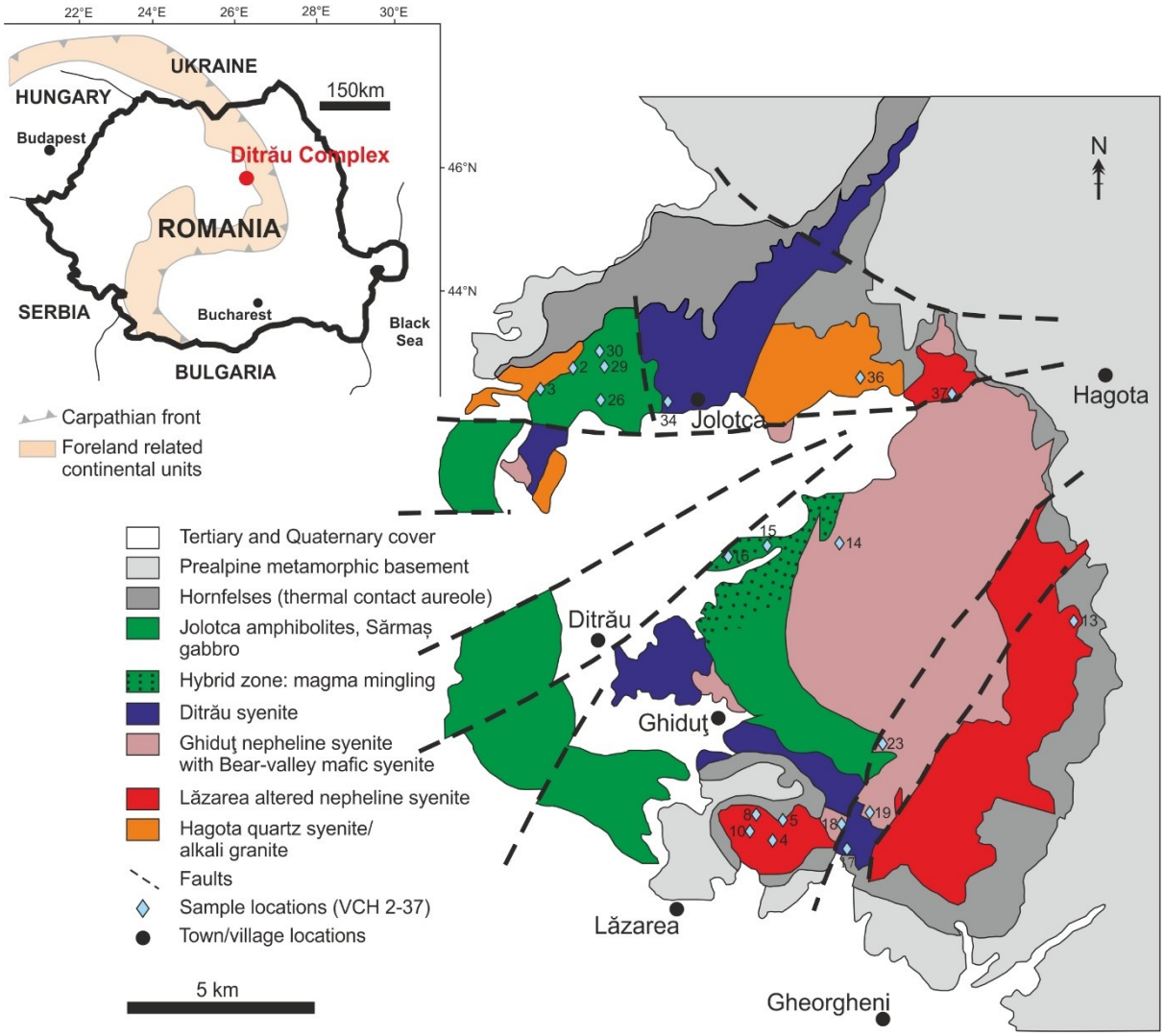

Figure 1. Simplified geological map redrawn after Jakab (1998), Krautner and Bindea (1998), Fall et al. (2007) and Batki (2009), with adaptions based on fieldwork observations and lithology nomenclature from this study. Only localities where samples were collected are denoted. Inset shows the position of the Ditrău Complex in Romania.

Table 1. A summary of previous lithology names from the literature, compared to the new lithodemic classification provided by this paper.

Unit name in literature	This paper	Reference
-	Jolotca amphibolite	-
Alkali gabbro I	Sărmaș gabbros	Morogan et al., 2000; Fall et al., 2007
Alkali diorite	Bear-valley mafic syenite	Morogan et al., 2000
Ditró essexites/mixed diorite-gabbro-syenite zone/Alkali gabbro II	Hybrid zone	Streckeisen, 1960/Morogan et al., 2000
Syenite-monzosyenite	Ditrău syenite	Krautner and Bindea, 1998 and Morogan et al., 2000
White syenite/Detroite/Nepheline syenite	Ghiduț nepheline syenite	Jakab, (1998)/Morogan et al., 2000; Fall et al., 2007
Red syenite/"red, hydrothermally altered variety" of nepheline syenite	Lăzarea altered nepheline syenite (LANS)	Jakab (1998)/Morogan et al., 2000
Quartz syenites	Hagota quartz syenite	Jakab, (1998); Morogan et al., 2000; Batki, 2009
Mafic dykes	Mafic dykes	Morogan et al., 2000
Mineralised veins hosted in a carbonate gangue	Mineralised veins	Săbău, 2009; Hirtopanu et al., 2010; Hirtopanu et al., 2013a

GEOLOGY OF THE COMPLEX

Previous work has focused on the age and petrogenesis of the igneous rocks and investigation of the mineralogy of the REE veins, but the relationships between the two have not been described in detail. This section lays out our current understanding of the structure of the Ditrău Complex, including the late REE veins, based on an assessment of all previous work and on fieldwork carried out during summer 2015. The Ditrău Complex is characterised by moderate topography, with rolling hills covered in grass and thick woodland. Outcrops are largely found in stream valleys, road cuts and old quarries, with boulder fields on hill tops providing additional geological information. The mineralised veins have previously been exploited but the adits are now closed; mine dumps therefore provide valuable specimens of the vein material.

The complex is exposed such that outcrops provide a transect from mafic-ultramafic cumulate rocks through to the highly evolved nepheline syenites and quartz syenites. Previous publications (Fall et al., 2007; Jakab, 1998; Morogan et al., 2000) have used a variety of unit names that are not consistent with observations made in the field during this study. Consequently, it has been necessary to propose a new set of lithological units (Table 1); the formal lithodemic classification for this work is based on non-genetic, descriptive field observations, supplemented by optical microscopy and previous literature. These units are described below and their distribution is shown on Fig 1.

Jolotca amphibolite

The most primitive lithology in the Ditrău Complex is the Jolotca amphibolite, a black, medium-grained, amphibole-dominated, locally foliated ultramafic rock found as discrete bodies in association with the gabbros and syenodiorites of the Jolotca region (Pál-Molnár et al., 2015). In situ exposures are typically highly weathered and take the form of eroded gullies. However, fresh Jolotca amphibolite can be observed in hand specimens at a number of mine waste dumps. Accessory minerals in the amphibolite include randomly oriented cumulus titanite, up to 1 cm long (Fig 2(a)). The amphibolites are commonly cut by <2 mm carbonate veins. In both outcrops and mine dumps the amphibolites are cross-cut by abundant 5–20 cm wide pegmatitic and aplitic syenite veins. Other ultramafic rocks, peridotites and pyroxenites, are reported by Morogan et al. (2000) but were not seen in this study.

Sărmaș gabbro

Sărmaș gabbros are exposed in the west of the complex and can be studied in the limited drill core held by the state and G. Jakab in Gheorgheni, Romania. They crop out in the Jolotca region in weathered gullies (similar to the Jolotca amphibolite); in fresher outcrops close to the town of Ditrău; and in a hybrid zone with Ditrău syenite (see below) to the east of the town of Ditrău. The freshest samples are found as blocks (10–80 cm) in mine waste dumps.

The coarse-grained gabbros within the Jolotca and Ditrău region are characterised by granular amphibole, plagioclase feldspar and titanite. Accessory minerals include magnetite, apatite and zircon. Medium-grained gabbros were observed in one outcrop in a quarry within the Jolotca region and are similarly massive and composed of amphibole, biotite, plagioclase and titanite. The gabbros have a variably present, weak foliation. This unit is comparable to the alkali gabbro I of Morogan et al. (2000) and Jakab's (1998) alkali gabbros seen in deep drill-cores across the complex.

In the Jolotca area a dimension stone quarry provides excellent exposures demonstrating magmatic processes (locality VCH-3; Supplementary Table 1). Multiple mafic enclaves c. 5–10 cm diameter are elongated to form parallel lenses, giving the outcrop a banded appearance. These enclaves were described as 'Alkali Gabbro II' by Morogan et al. (2000). The enclaves are surrounded by strongly foliated interstitial syenite (Fig 2(b)). There is a horizontal contact across which there is a rapid change from enclave-dominated to syenite-dominated. Across 2 m of stratigraphic height, the mafic enclaves disappear (from the 2D perspective visible in the quarry

cut). Observations from the quarry provide evidence of both magma mingling and deformation within the magma chamber.

Gabbro hybrid units

In the hybrid zone east of Ditrău, gabbros are cut by sheets and net-veins of coarse-grained nepheline syenite forming sub-angular to angular gabbroic enclaves, with sharp boundaries but no chilled or baked margins (Fig 2(c)). In a few places, gabbro-syenite contacts are diffuse over a few cm, with partially disaggregated enclaves. Locally within the enclaves, ultramafic (amphibolite) clots up to 10 cm in diameter occur. This zone shows significant variations in deformation state, with the magmatic textures grading, over hundreds of metres, into intensely foliated and deformed lithologies that are well-exposed in roadside outcrops (locality VCH-16; Supplementary Table 1). This intense deformation indicates active shearing within the magma chamber.

Streckeisen (1960) referred to the hybrid outcrops as 'Ditró essexites' (Table 1). Our observations indicate complex magmatic textures developing in a highly active magma chamber, with evidence for magma mixing and mingling, as proposed by Morogan et al. (2000). The evidence does not support Jakab's (1998) proposal that the 'essexites' were formed by metasomatism of country rock.

Ditrău syenite

The Ditrău syenite lies chiefly on the western side of the complex with good exposures in the Jolotca and Lăzarea areas. The Ditrău syenite is a mela-syenite, ranging from medium (1–5 mm) to coarse-grained (> 5 mm) and is dominated by tabular alkali feldspars, amphiboles (<1 cm wide), biotite, accessory euhedral titanite (<5 mm) and magnetite. The Ditrău syenite is heterogeneous, locally becoming more dioritic with increasing amounts of modal amphibole (comprising 15–40 % of the rock). Nepheline and HFSE-rich accessory minerals are notably absent. The syenitic texture varies from massive to foliated, with an igneous foliation defined by euhedral feldspars and amphibole. The lithology is cut by abundant aplitic veins (1–3 cm wide) and fine-grained mafic dykes. The Ditrău syenite as defined here encompasses the rock-types described as syenite-monzosyenite by Krautner and Bindea (1998) and Morogan et al. (2000).

Ghiduţ nepheline syenite

Nepheline syenites are dominant in the central and eastern areas of the Ditrău Complex, near to the village of Ghiduţ. The best exposures are in trial quarries, extensive road-cuts and the valley-side. The nepheline syenite is white and generally massive (Fig 2(d)). The modal mineralogy is spatially heterogeneous on the scale of tens of metres, and can grade into the Bear-valley mafic syenite (described below).

The Ghiduţ nepheline syenite is a granular, coarse-grained rock, characterised by medium-grained to very coarse-grained tabular, white alkali feldspars (<4 cm) and large (1–2 cm) grey, euhedral nepheline. Nepheline is locally altered to cancrinite, with yellow rims around nepheline crystals visible in hand specimen. Patchy blue sodalite typically follows 2–3 mm wide fractures, and is also found interstitial to the feldspars and nepheline. Amphibole and biotite are present (up to 20%) in medium-grained nepheline syenites, but not in the coarsest-grained varieties. The Ghiduţ nepheline syenite is equivalent to the 'Ditroite' and the white nepheline syenites (Table 1), described by Jakab, (1998), Morogan et al. (2000) and Fall et al. (2007).

A superb 40 m wide exposure was observed in a quarry lying adjacent to the track which cuts through the Ditrău Valley (locality VCH-14; Supplementary table 1). The outcrop has a well-defined set of steeply westward dipping fractures. A weathered biotite-filled dyke (0.3 m wide) cuts the Ghiduţ nepheline syenite parallel with the fractures (Fig 2(d)). The quarry exhibits a 20 m transition zone from fresh nepheline syenite to an altered variant surrounding the dyke. The Ghiduţ nepheline syenite in close proximity (<2 m) to the mafic dyke contains large biotites and zircons (up to 1 cm) and greenish mica aggregates replacing nephelines. Altered mafic dykes cutting the Ghiduţ nepheline syenite are common and this locality demonstrates that host rock alteration can be developed along the margins of the dykes.

Bear-valley mafic syenite

The Bear-valley mafic syenite is intimately associated with the Ghiduţ nepheline syenite, but exposure of mafic syenite is limited. Samples were collected in the centre of the complex and towards the Lăzarea region. The Bear-valley mafic syenite contains small amounts of nepheline, but is notably more mafic than the Ghiduţ nepheline syenite with greater than 35% mafic minerals. The mafic syenite is medium- to coarse-grained and generally has a foliation defined by mafic minerals. Xenoliths of amphibolite (2–4 cm in width) are found within the Bear-valley mafic syenite.

Lăzarea altered nepheline syenite (LANS)

The LANS predominates along the south-easterly margin of the Ditrău Complex. This unit has previously been named the 'Red syenite' (G. Jakab, 2015, pers. comm) and the "red, hydrothermally altered variety" of nepheline syenite (Morogan et al., 2000). Variation in the LANS can be well-studied in mine dumps on the eastern side of the intrusion (locality VCH-13; Supplementary Table 1; Fig 2(e)). Good exposures of LANS are rare, but small outcrops and mine dump material can be seen on the hills north-east of Lăzarea and along road cuts in the NE of the complex.

Grain size is variable, fluctuating from coarse- to very coarse-grained (5 to >10 mm respectively). The unit contains haematite throughout giving the characteristic red colour, but this colouration is not always indicative of, nor essential to, the LANS. The LANS is characterised by dull green pseudomorphs after nepheline (0.2–3 cm), large alkali feldspars (0.5–1 cm) and up to 15% mafic minerals (both biotite and amphibole). The proportion of mafic minerals decreases to 5% as crystal size increases. Molybdenite is found within the unit, generally along fractures, and is seen in association with fluorite in the east of the complex.

The LANS locally shows a pre-full crystallisation foliation which is defined by the mafic phases and is strongest in the medium-grained syenite, with moderate foliation in the coarse-grained syenite. The altered nepheline syenites are cut by a wide variety of later veins and fractures. The fractures are clearly visible in hand-specimen as they are generally red due to the presence of haematite (Fig 2(e)). Felsic veins (aplitic and pegmatitic), mafic veins (microdiorite to amphibolite), biotite-rich and sulphide-rich veins and carbonate veins, with an abundance of accessory minerals (e.g. zircon, pyrochlore, and apatite), 0.3–10 cm wide cut the foliation, often with haematised vein margins.

Sheets of LANS (~15 cm wide), extend out into the thermal contact aureole, cutting the country rock schist in a number of hill-top boulders in the Lăzarea area.

Hagota quartz syenite

Quartz syenites are found in the Jolotca area and north-east of the complex, as recognised by previous authors (Batki, 2009; Jakab, 1998; Morogan et al., 2000). They are massive, medium-grained granular rocks, comprised of alkali feldspar and quartz with accessory biotite. Alkali granites have also been described, but were not recognised during our fieldwork.

Mafic-ultramafic dykes

Fine-grained mafic dykes, including lamprophyres (15–50 cm wide; Batki, 2009) cut all major lithologies, excluding the Hagota quartz syenite. The dykes are black to dark grey and characterised by fine-grained feldspar (<5%) and amphibole. They are altered along their margins, with amphibole replaced by biotite (Fig 2(d)). This creates a characteristic 'friable' texture which extends variably to the centre of the dyke.

Mineralised veins

Mineralised veins with a carbonate gangue cross-cut mafic-ultramafic lithologies of the Ditrău Complex in the Jolotca region, and country rocks in the Belcina area. No in-situ outcrops have been found within the Jolotca region and therefore the characteristics described here are from mine dump samples. Jakab (2015, pers. comm.) describes the carbonate mineralised veins at Jolotca as typically 1 m wide, trending E-W, parallel with the

Jolotca valley and dipping 60˚N. Previous mineral exploration suggests that faulting has offset the veins (Jakab, 2015, pers. comm.).

A wide range of minerals has been described in these veins (Hirtopanu et al., 2015, 2013a, 2010; e.g. Jakab, 1998); of these rutile, monazite and pyrite were recognisable in hand specimens in the Jolotca area. The monazite gives the veining a red colouration, making it easy to identify in the field (Fig 2(f)). The veins in the Belcina area contain xenotime and thorite as well as sulfide minerals, and are highly radioactive. Samples could therefore not be obtained safely.

Structure of the Complex

Previous authors have suggested that the Ditrău Complex represents a ring intrusion (e.g. Morogan et al., 2000; Pál-Molnár, 2000; Pál-Molnár et al., 2015), although the presence of cumulate structures has been recognised (Morogan et al., 2000; Pál-Molnár et al., 2015). However, we consider that the field evidence is more consistent with emplacement in a broadly horizontal magma chamber that has subsequently been tilted towards the east. Although the Carpathian Cenozoic thrust systems are east-facing, the Bucovinian nappe has been folded during Cenozoic thrusting (Matenco et al., 2010), and the tilting of the Ditrău Complex may well be attributable to this folding. The mafic to ultramafic cumulates (the Jolotca amphibolite and Sărmaș gabbro) show clear banding and foliation dipping broadly eastward, and are considered here to represent the original lower part of the magma chamber. The evidence of extensive hybridisation in the central part of the magma chamber (gabbro hybrids) indicates more highly evolved magmas mixing and mingling with the mafic crystal mush. The Ghiduţ nepheline syenite represents the most highly evolved magmas in the upper part of the chamber, with the LANS representing an intensely altered roof zone.

A zone of deformation transects the complex, running NE from the town of Ditrău. Much of this zone is covered by younger sediments, but where outcrops are exposed the gabbros and gabbro hybrids are seen to be strongly deformed, near-mylonitic. Relatively undeformed syenitic veins cut across this deformation fabric, indicating that the fabric formed within the magma chamber. The high-temperature deformation within these outcrops most likely indicates a zone of active shearing within the magma chamber, which has been subsequently reactivated by later faulting. Brittle faults and fractures are common within the complex.

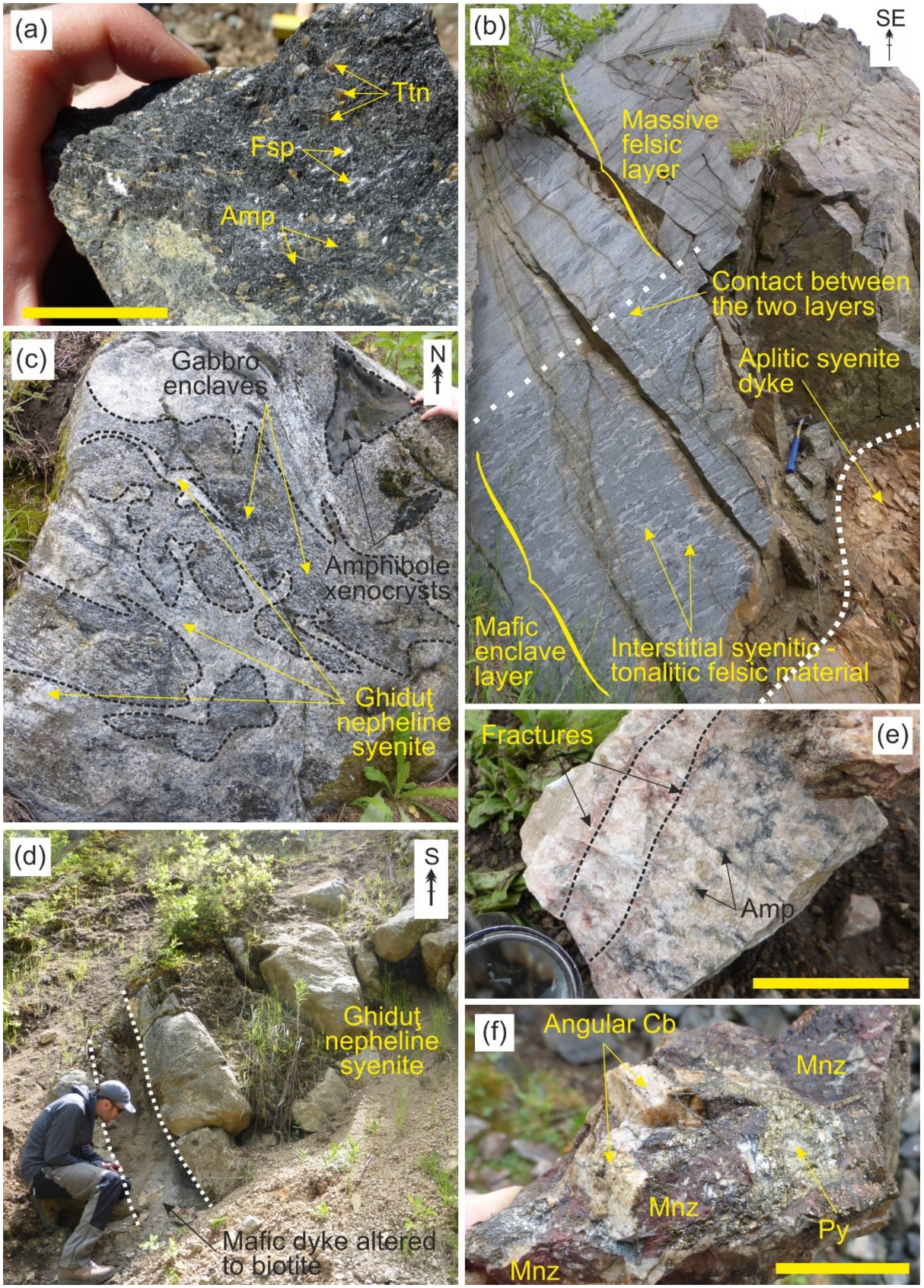

Figure 2. Field photos from the Ditrău Complex. (a) Jolotca amphibolite hand specimen containing large titanite crystals; (b) magma mingling in the Jolotca region, note the mafic enclaves; (c) magma mingling in the Ditrău valley between Ghiduţ nepheline syenite and Sărmaş gabbro, with Jolotca amphibolite xenocrysts; (d) altered mafic dyke cutting the Ghiduţ nepheline syenite in the Ditrău valley; (e) Lăzarea altered nepheline syenite with fractures defined by red minerals, sampled in the Lăzarea region; (f) mineralised vein hosting monazite and pyrite in a carbonate gangue taken from an adit waste dump in Jolotca. Mineral abbreviations used in photos are taken from Whitney and Evans, (2010).

SAMPLES AND ANALYTICAL METHODS

We collected forty-six samples from thirty-eight localities in the complex, representing all the key lithologies (Supplementary Table 1). Fieldwork focused on two key areas: (1) the Jolotca region in the north-west, and (2) the southern area of the Ditrău Complex. The samples covered a range of lithologies and alteration products. Samples were characterised at the British Geological Survey, Keyworth using a Zeiss Axioplan 2 imaging microscope and two SEMs for semi-quantitative mineral compositions, element EDS X-ray maps and back-scatter electron (BSE) imagery: (1) an FEI Company Quanta 600 environmental scanning electron microscope (ESEM) equipped with an Oxford Instruments INCA Energy 450 energy-dispersive X-ray microanalysis system (EDXA), set to 20 kV at 1.2 nA, with a working distance of 10 mm; and (2) a LEO 435VP variable pressure digital SEM, using Oxford Instruments INCA EDXA system, set to 20 kV at 0.5 nA and a working distance of 19 mm.

Twenty rock powder samples were prepared using a chrome steel jaw crusher and ground using an agate milling vessel. At each stage the crushed sample material was split using a riffle splitter. Whole rock analyses for major elements were obtained by fused bead XRF quantitative analyses undertaken by PANalytical at the British Geological Survey, Keyworth. The analyses were conducted using a PANalytical Axios sequential fully automatic wavelength-dispersive X-ray fluorescence spectrometer. Loss on ignition (LOI) ranges from 0.4–3.6% with final totals all within the range 99–101%.

Whole rock analyses for a suite of fifty-four minor and trace elements were obtained by Inductively Coupled Plasma Mass Spectrometry (ICP-MS) using dissolution by Na-peroxide fusion to ensure resistant accessory minerals were fully digested. ICP-MS analysis was carried out at the BGS, Keyworth, on an Agilent 7500cx series machine, which was calibrated using known concentrations in solution of all the elements for analysis. Overall, the two duplicate pairs indicated the results had good precision: the trace elements of interest (Hf, U, Th, Mo, Sr, Y, Zr, Nb, REE, and Ta) have a relative percentage difference typically below 10% between duplicate sample pairs. Sm, Eu, Ho and Mo have a slightly higher relative percentage difference of between 10% and 20%. Four certified reference materials (CRMs) of varying composition (syenite powder, GSR-7; andesite, AGV-2; Columbia River basalt, BCR-2; and diorite gneiss, SY-4) were analysed. All trace elements of interest were within 10% of certified reference values, except for U, Th, Ta, Gd and Zr, which were within 15%.

Apatite compositions were measured using a Cameca SX100 electron microprobe equipped with five wavelength-dispersive spectrometers at the Grant Institute of Earth Science, University of Edinburgh. Two analytical condition routines were run: a light element analysis first followed by a heavy element analysis. The instrument uses Cameca's PeakSight software, with ZAF correction. The light element analytical routine was run at 20 kV, 10 nA with a 12 µm defocused spot to analyse: F, Cl, Na, P and Ca. Na was measured for 60 s on peak, the rest for 20 s. Volatile analysis time was minimised to reduce volatisation of the elements and migration of F and Cl. These conditions have been previously identified as minimising the potential for halogen migration during apatite analysis by EPMA (Stock et al., 2015; Stormer et al., 1993). A synthetic spectrometer crystal (PC1) was chosen specifically for F due to its greater stability than natural spectrometer crystals. The heavy element routine was run at 20 kV, 80 nA with 12 µm spot to analyse: Al, Si, S, Mn, Sr, La, Y, Ce, Fe, Pr, Nd and Y. Mn was measured for 90 s on peak, Sr for 20 s, Ce for 30 s, Y for 120 s and the rest for 60 s. Oriented apatite secondary standards (Durango and Wilberforce) were run and had good precision with two standard deviations below 0.5 for Durango and below 1.0 for Wilberforce for all elements analysed over the duration of all the analyses. The two standard deviations relative percentage for the unknowns is below 5% for F, P, Ca, Si and Ce; below 10% for Mn, Sr, La, Y, Fe and Nd. It is 42% for Pr. Na, Cl, S and Pr reach concentrations 3.3 times detection limit in selected lithologies. Over 280 apatite analyses were performed, mostly from apatite cores, on eight different samples. The apatite analysis totals have been recalculated accounting for mixing on the monovalent anion sites (e.g. F^-, Cl^- and OH^-). Many of the apatite analyses reported low totals; this is likely due to the presence of unmeasured HREE in the apatite structure.

RESULTS

Petrography

Jolotca amphibolite

The Jolotca amphibolites are coarse-grained rocks, characterised by amphibole, titanite, biotite, plagioclase feldspar, apatite, and pyrite. The major minerals are generally > 0.5 mm (Fig 3(a)). Mafic phases account for >80% of the amphibolite. Large green amphiboles (hornblende) are euhedral to subhedral, ranging from 1–7 mm across; there is internal zoning within the smaller amphiboles (<1 mm). Locally, amphibole crystals show a preferred alignment, defining a foliation. The amphibole rims are typically altered to biotite. Plagioclase feldspars (1–2 mm) are interstitial, comprising <20% of the amphibolite. Apatites are euhedral to subhedral and relatively homogeneous, forming both equant and acicular habits (up to 1 mm in length). The euhedral, homogeneous apatites in this lithology are referred to hereafter as Ap_{JA}, this corresponds to the apatites selected for EPMA. Apatite also forms inclusions within amphibole and plagioclase. Euhedral titanites (1–2 mm) contain inclusions of apatite and small (<50 μm) sulfide inclusions. Disseminated pyrite is present as 100–500 μm euhedral crystals that contain inclusions of apatite and are fringed by biotite crystals. The Jolotca amphibolite is cut by thin (100–200 μm) sulfide and carbonate veins which transect all mineral phases. The sulfide veins are dominated by subhedral pyrite crystals; the carbonate veins are calcite dominated.

Sărmaș gabbro

The Sărmaș gabbros are phaneritic cumulate rocks comprising plagioclase, pyroxene, amphibole, biotite, titanite and apatite, and have been described in detail by Morogan et al. (2000). The gabbro generally has >60% mafic minerals (largely amphibole, with smaller amounts of pyroxene and biotite) and locally shows cumulus layering, alternating between mafic-rich and feldspar-rich layers, 1–2 mm thick. Titanites up to 1.5 mm are common; they are euhedral and host ubiquitous apatite inclusions. Apatites and opaque oxides (dominated by titanomagnetite) are common accessory minerals.

Bear-valley mafic syenite

The Bear-valley mafic syenite comprises feldspar (perthitic microcline), < 15% nepheline, amphibole and titanite. The mafic mineral phases are typically 0.3–1 mm across, while euhedral titanite crystals are smaller (0.1–0.5 mm), as are apatite grains (<0.1 mm). Titanite comprises ~5% of the rock but inclusions of apatite are very rare.

Ditrău syenite

The Ditrău syenite varies from medium- to coarse-grained, depending on its spatial position within the complex. Tabular feldspars, up to 2 mm in length, comprise >85% of the rock and alignment along their c-axes commonly defines a foliation. Orthoclase and microcline dominate with <10% plagioclase feldspar; the alkali feldspar internal grain boundaries are undulose. Ferromagnesian minerals comprise <10% of the total phases; subhedral amphiboles are the major mafic mineral, and are typically c. 0.5 mm across with associated biotite flakes up to 0.6 mm long. Euhedral accessory minerals are titanite, apatite and zircon. These occur along alkali feldspar grain boundaries and as inclusions within the feldspars. Titanite has a lower modal abundance than in the Jolotca amphibolite or Sărmaș gabbro, and smaller crystal sizes (up to 0.6 mm). Zircon crystals range from 0.3–0.5 mm. Alkali feldspars show limited alteration to sericite, which is generally constrained to the feldspar cores.

Ghiduț nepheline syenite

The Ghiduț nepheline syenite is a coarse-grained rock composed largely of subhedral alkali feldspar and nepheline (Fig 3(b)). Alkali feldspar (orthoclase, microcline and perthite) forms large plates typically up to 3 mm (locally > 5 mm), set in an alkali-feldspar rich groundmass with crystals < 1 mm diameter. The large plates have undulose grain boundaries and no preferred orientation. Nepheline also forms large, subhedral crystals up to 3 mm in size. Plagioclase feldspar laths (50–200 μm wide) occur in the groundmass and make up <8% of the rock. Mafic phases are subhedral and include Na-amphiboles (arfvedsonite; c. 0.5 mm in diameter) and biotite

(0.3–0.6 mm). The Na-amphiboles have inclusions of thorite and magnetite (<10 μm) distributed uniformly across the crystals, and in the rims thin (0.1 mm) albite and orthoclase inclusions. Randomly oriented xenoliths of ultramafic rock (2 cm in diameter) are locally present. They are dominated by pyroxene, amphibole and biotite, with <10% leucocratic material.

Large euhedral zircons, up to 3 mm in diameter, are common. The zircons have internal zoning and multiple inclusions, and based on petrological observation across the lithology, two zircon zones are recognised: (1) an inclusion free zone, commonly forming the zircon core; and (2) a heterogeneous zone with multiple inclusions of varying sizes (<20–300 μm). This can be a single zircon or form a rim around a type (1) zone. The type (2) zones contain several inclusion types: tabular albite inclusions (>50 μm long) which are continuous with the surrounding matrix near the zircon rim; and inclusions (typically <50 μm) of LREE, Y, Th and/or Nb bearing phases such as pyrochlore, thorite, zirconolite, and monazite.

Disseminated euhedral pyrites (0.2 mm wide) and a small amount of molybdenite are present throughout, but ilmenite and magnetite are the dominant oxides within the Ghiduţ nepheline syenite. They form composite grains with sharp internal grain boundaries between phases, but where magnetite is absent, ilmenite is skeletal, ranging in diameter from 0.1–0.4 mm. Massive ilmenite reaches 0.6 mm. Ilmenite and rutile are associated with globular pyrochlore, which forms patches c. 0.2 mm wide, hosting Nb-Mn-Ti-rich inclusions. Accessory euhedral titanites (0.3–0.8 mm) are also rarely present.

The Ghiduţ nepheline syenites show evidence of progressive alteration of the original magmatic mineral assemblages. This is characterised by increasing alteration of nepheline, recrystallization of feldspar, increased presence of perthite, and introduction of sodalite both around nepheline rims and in fractures. This alteration is particularly evident in areas around biotite-rich mafic dykes.

Nepheline alteration in the Ghiduţ nepheline syenite is variable and can be separated into two phases. The first phase is alteration of nepheline to cancrinite, which forms stubby crystals that grow in from the margins of the nepheline crystals (Fig 3(c)). Sodalite, muscovite, pyrochlore and opaque oxides (e.g. magnetite, ilmenite) occur between the cancrinite crystals. In some crystals cancrinite has replaced nepheline entirely, but has not replaced the alkali feldspar inclusions, as observed by Fall et al., (2007). The second phase is a fine-grained muscovite aggregates replacing both nepheline and cancrinite. Within the Ghiduţ nepheline syenite this texture is poorly developed, occurring locally within nepheline cores. The two types of nepheline alteration can co-exist within a single nepheline crystal, with muscovite alteration more common in the core and cancrinite more common along the grain boundaries.

With progressive alteration, larger plates of alkali feldspar show recrystallization to albite at their rims (swapped rims) and development of patchy perthite textures (Fig 3(d)). Such textures are indicative of late-stage fluids controlling recrystallization within the syenite (Parsons, 1978).

Alteration textures around Na-amphiboles (arfvedsonites) are common in the same samples that show nepheline alteration to cancrinite. Subhedral arfvedsonites (1–3 mm) have characteristic diamond shapes with embayment textures along their undulating boundaries (Fig 3(e)). Arfvedsonites in proximity to nepheline (<1 mm) have a rim of compositionally homogeneous albite laths (0.2–0.3 mm) growing perpendicular to the arfvedsonite boundary and pseudomorphing the primary euhedral shape. Within the well-defined albite rim there is a band of oxides, dominated by euhedral magnetite (50 μm wide), with small (<10 μm) bleb-like inclusions of thorite. Anhedral orthoclase and pyrochlore crystals (50–100 μm wide) lie within the albite rims. Between nepheline and albite there is a thin rim (<50 μm thick), which is low in K and Si, but enriched in Na and Ca. This texture is attributed to a reaction between Na-amphibole and nepheline in the presence of a fluid.

At the quarry where the biotite-rich mafic dyke cuts the Ghiduţ nepheline syenite, intense alteration occurs in the nepheline syenite around the dyke. Amphibole has been replaced by large biotites (Fig 3(f)). The nepheline has been completely altered to micaceous aggregates and/or cancrinite, similar to the textures in the LANS (see

below). Nepheline inclusions within perthite have been completely replaced by muscovite and/or cancrinite. Perthite plates show undulose internal grain boundaries and extensive recrystallisation to albite at the margins.

Lăzarea altered nepheline syenite (LANS)

The LANS is medium- to coarse-grained, with patchy variation in grain size between localities. The characteristic feature is complete alteration of original nepheline crystals to a micaceous aggregate (i.e. liebnerite; Fig 4(a)). These nepheline pseudomorphs are up to 5 mm across and retain their euhedral shape. The other major mineral is perthitic alkali feldspar, forming subhedral to anhedral crystals up to 3 mm long, which are locally sericitised and recrystallised. Plagioclase feldspars are rarely present. The main mafic minerals are amphibole and chloritised biotite, which typically form mafic clots 1–2 mm across, these comprise less than 10% of the rock. These clots commonly contain apatite, titanite, sulfide, zircon, epidote group minerals and carbonate minerals. Apatite crystals (20–150 μm) are heterogeneously distributed through the lithology. Regardless of textural context, the apatites are anhedral to euhedral and named Ap_{LANS}. Rare apatite and subhedral zircon crystals, typically up to 0.4 mm diameter, occur along feldspar grain boundaries. Euhedral pyrites (20 μm) are disseminated through the LANS.

Fracture infills up to 1 mm in width are very common and generally are zircon-rich, with some monazite and pyrochlore (<100 μm). The monazite and pyrochlore generally has patchy internal zonation. The zircons (up to 1 mm diameter) are euhedral to anhedral and contain inclusion-rich zones. Thorite inclusions are spread throughout the zoned zircons whilst Ca-rich inclusions are observed near the zoned zircon's rim. Other common phases in the fracture infills are monazite, magnetite, pyrochlore, allanite, and LREE-carbonates (bastnäsite). Overall, HFSE-bearing accessory minerals are more abundant in the LANS than in other lithologies within the Ditrău Complex.

A variety of late veins cross-cut the LANS. Aplitic veins (0.5–5 cm wide) are dominated by fine-grained albite and orthoclase, and have accessory subhedral to anhedral apatite crystals, varying from 20–100 μm (Ap_{APLITE}). The apatites occur dispersed along grain boundaries of albite and orthoclase, as inclusions in albite, and associated with the margins of mafic clots and altered nephelines within the aplitic vein. The apatites are generally larger in the centre of the veins.

Biotite-rich veins, up to 1 cm wide, comprise brown-yellow pleochroic subhedral biotite laths and subhedral albite (up to 0.5 mm) which make up >85% of the vein. Biotite defines a very clear foliation parallel with the vein margin (Fig 4(b)). Accessory phases include euhedral–subhedral apatite (50–200 μm), altered and unaltered subhedral titanite, and magnetite, titanomagnetite and muscovite. Apatite (Ap_{BV}) comprises c. 8% of the biotite-rich vein and chiefly occurs at feldspar and biotite boundaries, with the c-axis aligned with the igneous foliation. There are rare apatite inclusions within biotite. Towards the vein margins the accessory phases decrease in size and abundance, and biotite becomes increasingly anhedral. Zircon is associated with the vein margins.

Pyrite veins with associated sphalerite vary from 0.1–2 cm wide. The larger pyrite veins are surrounded by mica-filled fractures within feldspars and feldspathoids. The pyrite is also fractured and altered to iron oxide along the margins. Unlike the mineralised veins of the Jolotca region, the pyrite veins cutting the LANS do not have associated REE-phosphate mineralisation or carbonate gangue.

Carbonate veins cut all other veining and are present at the micron and hand specimen scale. The carbonate generally has 120° internal grain boundaries. The coarse-grained, equigranular carbonate veins (>10 cm in width) host large subhedral to euhedral apatites (up to 2 mm in diameter), which tend to cluster together with their c-axis aligned parallel to the vein margin (Fig 4(c)). Many have altered rims and some have carbonate inclusions (10–200 μm diameter) within their rims. The smaller apatites have a greater degree of alteration. Zircon is found along the margins of the carbonate veins.

Hagota quartz syenite

This is a medium grained, equigranular rock, dominated by alkali feldspar and <10% plagioclase feldspar. Subhedral feldspars range from 0.3–0.8 mm in diameter, rare larger grains (~1 mm) have perthitic textures. Interstitial quartz grains, generally >0.5 mm across, form c. 15% of the rock. Some of the feldspars have undergone secondary alteration to sericite. Anhedral altered amphibole has <7% modal abundance and is associated with rare anhedral biotite crystals and occasional euhedral titanite crystals (<200 μm wide). Small zircons (0.2–0.5 mm in width) occur along feldspar and quartz grain boundaries.

Mineralised veins

The mineralised veins of the Jolotca region are dominated by monazite (a key REE ore mineral at Ditrău), allanite, bastnäsite, rutile, molybdenite and sulfides (chiefly pyrite) within a carbonate gangue. Other minerals that have previously been recognised in these veins include chevkinite, cerite, columbite, euxenite, aeschynite, parisite, synchysite and thorite (Hirtopanu et al., 2015, 2013b, 2010). The bastnäsite forms crystals up to 300 μm wide with a weak preferred orientation along their c-axis. Large (0.1–1 cm diameter) aggregates of monazite (Fig 4(d)) host inclusions of thorite and zirconolite and contain interstitial molybdenite between individual, tabular monazite laths. The monazite aggregates are adjacent to massive pyrite (>3 mm), sphalerite (up to 2 mm) and galena. The pyrite contains ubiquitous apatite inclusions (Ap_{PY}); inclusions of monazite (c. 0.2 mm long) concentrated within the margins of the pyrite; and inclusions of carbonate, galena and chalcopyrite within the very outer limits of the pyrite rim (Fig 4(e)). Sphalerite contains small inclusions of galena and pyrite (<50 μm).

LREE-carbonates, phosphates and silicates (e.g. allanite, apatite up to 100 μm, and chlorite) are typically associated with the grain boundaries of monazite (Hirtopanu et al., 2010), particularly where the monazite is in contact with fine-grained calcite. Allanite also forms thin veins (c. 100 μm wide) cutting across the monazite aggregates. There are three distinct apatite populations in the mineralised veins: (1) apatite associated with allanite (Ap_{ALN}); (2) apatite associated with pyrite (Ap_{PY}); and (3) large homogeneous apatite (up to 300 μm diameter), which are observed solely within the carbonate gangue (Ap_{MV}; Fig 4(f)). The apatite inclusions within the large pyrite grains range from 100–500 μm in diameter and form distinct apatite inclusion zones. The apatite grains nearest the pyrite rim have a globular morphology and are inclusion-free, whereas the Ap_{PY} closer to the core of the pyrite grain themselves contain REE-enriched inclusions. These inclusions are subhedral and typically elongated parallel to the c-axis of the apatite.

The large apatite grains (Ap_{MV}) are distributed throughout the carbonate, although with a greater abundance adjacent to laths of monazite, which is also hosted in the carbonate gangue. Inclusions within Ap_{MV} are rare, but where present in the larger apatites, they are LREE-enriched; HREE-enriched inclusions were not observed. REE-bearing inclusions were not found in Ap_{ALN}.

Hirtopanu (2013a) describes the carbonate gangue as including ferrodolomite, ankerite, siderite and calcite. At least two carbonate gangue phases are recognised within the mineralised veins at Jolotca in this study: (1) fine-grained (<50 μm) calcite containing laths of monazite, euhedral pyrite, apatite, allanite, rutile and bastnäsite (Fig 4(f)); and (2) a coarse-grained calcite, with 120° internal grain boundary angles. Type (2) forms multiple veinlets (0.5–3 mm wide) with sharp boundaries, which cross-cut all other phases within the mineralised veins.

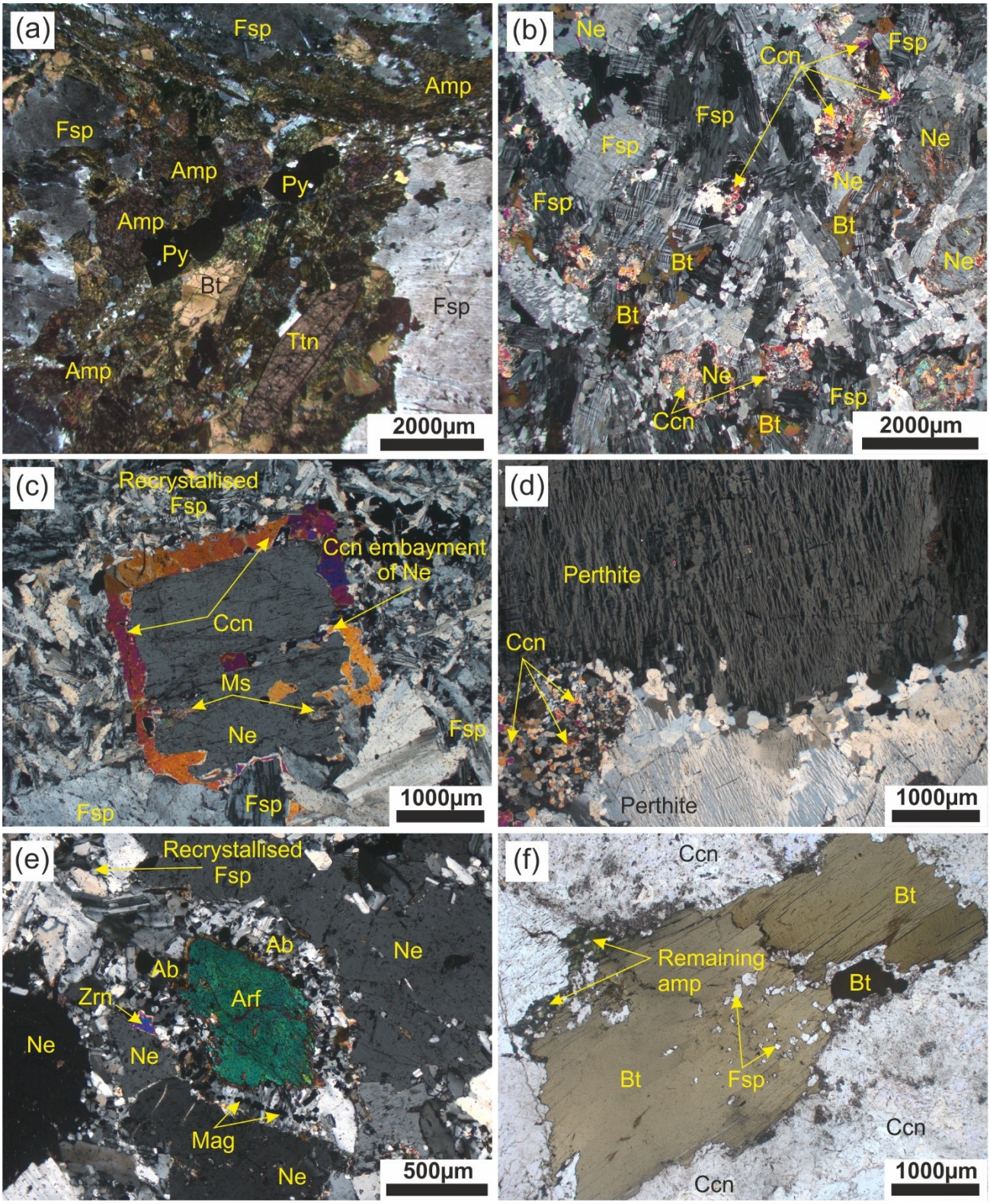

Figure 3. (a) XPL photomicrograph of Jolotca amphibolite showing a large titanite with apatite inclusions associated with amphibole and biotite. The mafic phases are cut by a pyrite-rich vein; (b) An XPL overview of the Ghiduţ nepheline syenite mineralogy, size, shape and textural relationships of the alkali feldspars, nepheline, cancrinite and biotite; (c) XPL photomicrograph of nepheline lath alteration and replacement by cancrinite, forming a 200µm rim; (d) XPL photomicrograph of alteration of the Ghiduţ nepheline syenite adjacent to a mafic dyke, showing albitisation of perthite plates, with adjacent cancrinite; (e) Reaction texture, in XPL, between nepheline and arfvedsonite, albite laths surround the Na-amphibole, with euhedral magnetite within the albite, note the zircon on the edge of the albite rim; (f) XPL photomicrograph of alteration of the Ghiduţ nepheline syenite adjacent to a mafic dyke showing biotite with remaining traces of amphibole on the edge and feldspar inclusions. Mineral abbreviations used in photomicrographs are taken from Whitney and Evans, (2010).

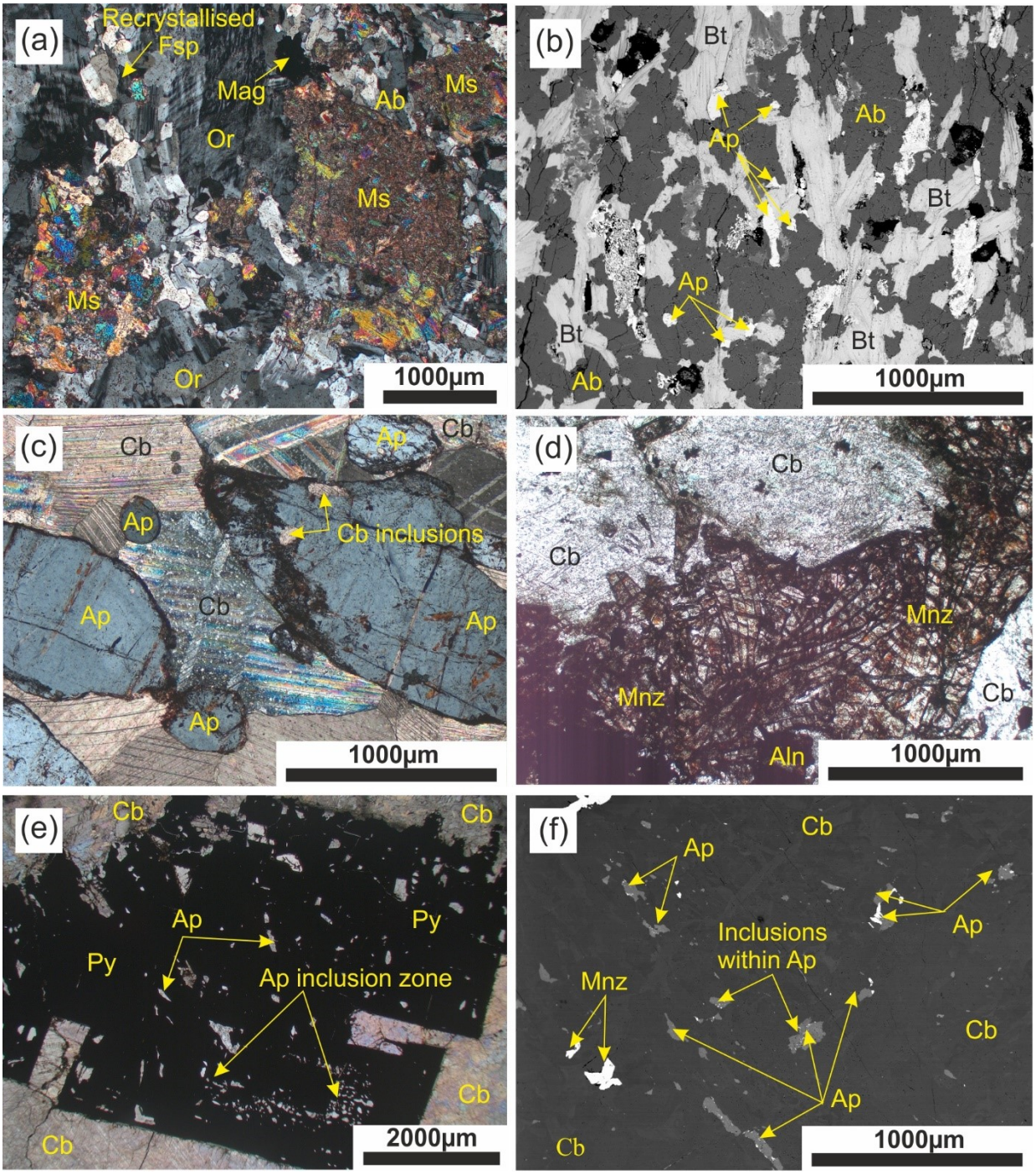

Figure 4. (a) The Lăzarea altered nepheline syenite in XPL, showing several muscovite pseudomorphs of nepheline laths surrounding recrystallized feldspar; (b) Textural association of apatite in a biotite-rich vein, <5mm, cutting the Lăzarea altered nepheline syenite, BSE image; (c) Textural association of apatite accessory phases in a carbonate vein cross-cutting the Lăzarea altered nepheline syenite in XPL; (d) PPL photomicrograph of coagulations of monazite laths surrounded by carbonate gangue within the mineralised veins; (e) BSE image of apatite inclusions within pyrite within the mineralised veins; (f) BSE image of apatite in the carbonate gangue of the mineralised veins. Mineral abbreviations used in photomicrographs are taken from Whitney and Evans, (2010).

Whole rock geochemistry

Major and trace element data of the magmatic lithologies in the Ditrău Complex are given in Table 2. SiO_2 ranges from 39.88 to 66.29 wt. % representing the magmatic evolution of the complex from Jolotca amphibolite to Hagota quartz syenite. It is important to note that many of the rocks of the Ditrău Complex have formed through cumulate processes and have undergone late alteration, so the composition of these rocks may not directly reflect the composition of their parental magma. The mineralised veins have not been analysed for whole-rock geochemistry, since their mineralogy is too heterogeneous to obtain a representative sample.

Harker plots show that $Fe_2O_{3\ total}$, Mn_3O_4, TiO_2, MgO, and CaO show a negative correlation with SiO_2 (Fig 5(a–e)). Total Fe_2O_3 attains a maximum of 13.59 wt. % in the Jolotca amphibolite, but is low in the syenites (c. 2 wt. %). Similarly, the Jolotca amphibolite, Sărmaș gabbro and Bear-valley mafic syenite have elevated TiO_2 concentrations, up to 3.73 wt. %, whilst the syenitic rocks contain less than 0.64 wt. %. These variations are consistent with fractionation of amphibole and titanite (cumulus phases in the Jolotca amphibolite) from an alkali basaltic parental magma. Magnesium numbers (calculated as 100*(Mg/(Mg+Fe))) range from 27 for the deformed Sărmaș gabbro to 2 for the Ghiduţ nepheline syenite; indicating genesis from an evolving magma through the complex. Likewise, CaO is highest in the mafic lithologies, up to 10.97 wt. % in the Jolotca amphibolites, and decreases with increasing SiO_2. For the more felsic lithologies CaO is typically below 3 wt. % and is negligible within the LANS.

K_2O concentrations show an overall weak positive correlation with SiO_2, ranging from 1.94 wt. % in the Jolotca amphibolite to a maximum of 7.64 wt. % in the LANS. The Ghiduţ nepheline syenite samples have a wide range of K_2O values (2.55–6.24 wt. %), which correlates with varied amounts of alteration that primarily occurs adjacent to cross-cutting mafic dykes. The altered Ghiduţ nepheline syenite adjacent to the mafic dykes has a lower K_2O concentration (0.72 wt. %), whilst the dykes themselves have relatively high K_2O concentrations of 3.97 wt. %.

Na_2O concentrations correlate positively with SiO_2 up to 55 wt. % SiO_2, above this point a notable divergence is observed in the syenites (Fig 5(f)). The Ghiduţ nepheline syenite has high Na_2O (7.31 to 12.94 wt. %), whilst the LANS has relatively low Na_2O values of 5.17–6.53 wt. %. The syenites of the Ditrău Complex have a negative correlation between K_2O and Na_2O contents (Fig 6), which can be related to initial fractionation of alkali feldspar and accumulation of nepheline in the most evolved syenitic lithologies, followed by alteration of nepheline to micaceous aggregates, indicating introduction of K_2O in fluids.

Al_2O_3 values are high across the complex, ranging from 17 wt. % in the Hagota quartz syenite to 23 wt. % in the Ghiduţ nepheline syenite. These values are comparable to alkali intrusions in Malawi, where nepheline syenites range from 16–24 wt. % Al_2O_3 (Eby et al., 1998) and are also comparable to previously published whole-rock data for the Ditrău Complex (Morogan et al., (2000). The Harker plot for Al_2O_3 has a concave trend, with an inflection at 58 wt. % SiO_2 indicating the onset of alkali feldspar crystallisation (Fig 5(h)).

Total alkali contents (Na_2O + K_2O), are generally high throughout the complex (between 5.11–15.36 wt. %; Table 2). The lithology with the lowest total alkalis and SiO_2 content is the Jolotca amphibolite (Fig 7). The total alkali content reaches a maximum of 15.36 wt. % in the Ghiduţ nepheline syenite, which lies within the nepheline syenite field and is distinct from the LANS and Ditrău syenite. These two lithologies plot along the nepheline syenite–syenite boundary with similar SiO_2 values and total alkali contents (c. 12 wt. %). The Hagota quartz syenite lies towards the alkali granite field with the highest SiO_2 content of 66.29 wt. %. Overall, the total alkali-silica plot shows evidence of a split fractionation trend within the Ditrău Complex, associated with the separate evolution of silica-undersaturated (Na-rich) and silica-saturated (more K-rich) magmas (Fig 7). The higher levels of SiO_2 in the Hagota quartz-syenite may be indicative of some crustal contamination of the magmas.

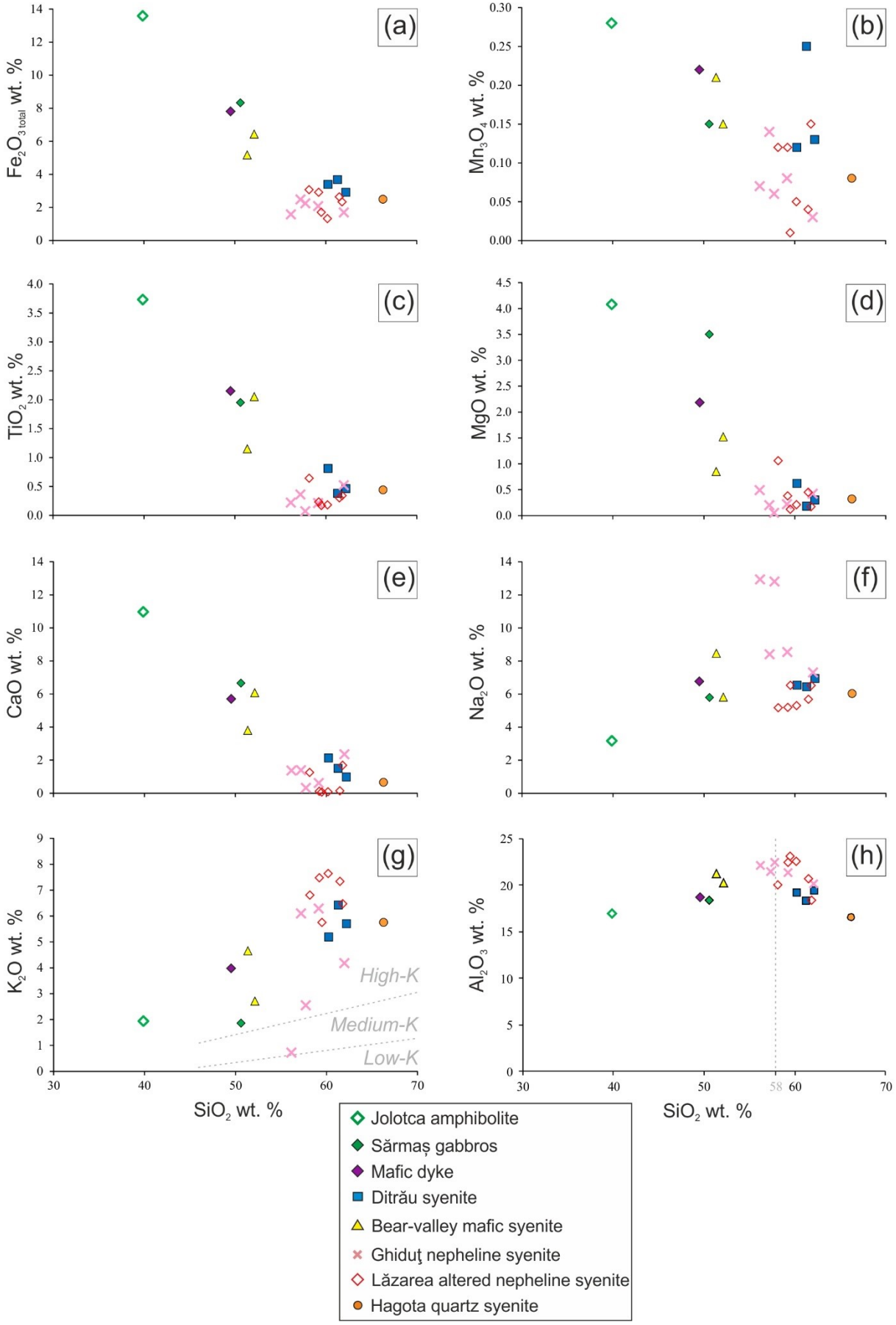

Figure 5. Harker variation diagrams for the Ditrău Complex.

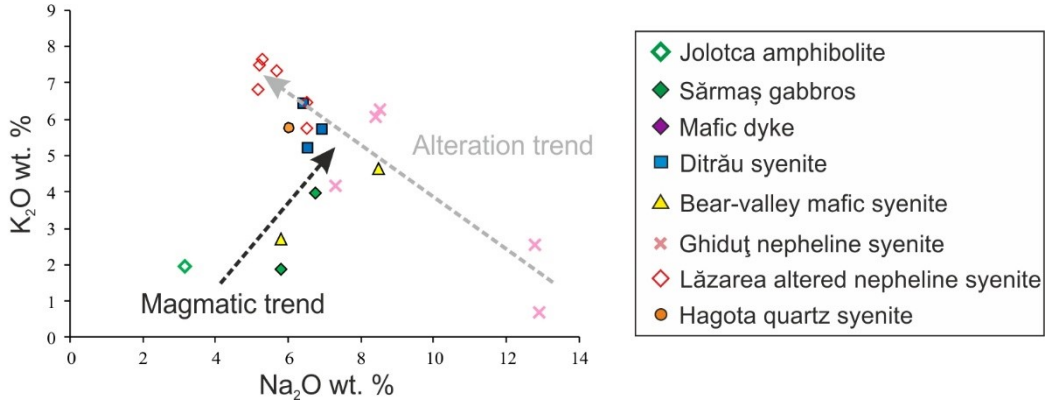

Figure 6. Plot of Na2O wt. % against K2O wt. % for the Ditrău complex. The black arrow shows the magmatic trend, whilst the grey arrow shows the alteration trend between the Ghiduţ nepheline syenite and the Lăzarea altered nepheline syenite (LANS).

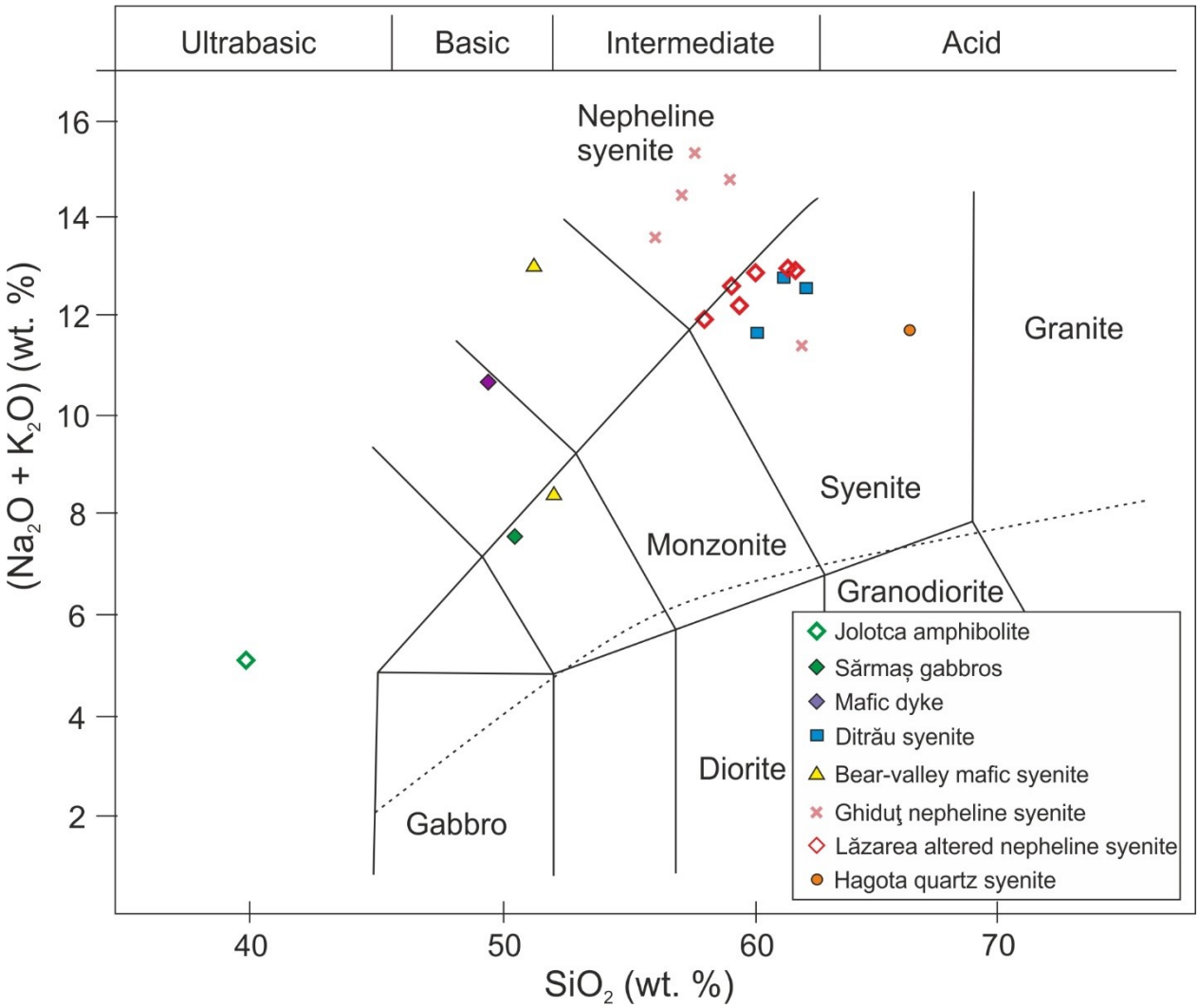

Figure 7. Plot of total alkalis versus silica for the sampled lithologies of the Ditrău Complex. Fields from Gillespie and Styles (1999). Dashed line represents boundary between alkalic rocks above and subalkalic rocks below (Miyashiro, 1974).

Table 2. Whole rock major and trace element data. Lăzarea altered nepheline syenite is abbreviated to LANS.

Sample number	**DJ01**	**DL34**	**DD30**	**DD22**	**DL32**	**DJ44**	**DD29**
Rock type	Jolotca amphibolite	Mafic dyke (Sărmaș gabbro)	Deformed Sărmaș gabbro	Ditrău syenite	Ditrău syenite	Ditrău syenite	Bear-valley maifc syenite
Majors	*wt. %*	*wt. %*	*wt. %*	*wt. %*	*wt. %*	*wt. %*	*wt. %*
SiO_2	39.88	49.53	50.61	61.3	62.2	60.24	52.14
TiO_2	3.73	2.15	1.95	0.38	0.46	0.81	2.05
Al_2O_3	16.93	18.75	18.36	18.28	19.32	19.14	20.21
Fe_2O_3 TOTAL	13.59	7.81	8.33	3.68	2.91	3.39	6.43
Mn_3O_4	0.28	0.22	0.15	0.25	0.13	0.12	0.15
MgO	4.08	2.18	3.5	0.18	0.3	0.62	1.52
CaO	10.97	5.69	6.66	1.5	0.98	2.13	6.08
Na_2O	3.17	6.76	5.79	6.44	6.94	6.54	5.81
K_2O	1.94	3.97	1.86	6.42	5.7	5.19	2.71
P_2O_5	1.74	0.63	0.49	0.03	0.06	0.12	0.4
LOI	1.94	1.29	1.04	1.18	0.44	0.55	1.02
Total	99.06	99.35	99.21	99.74	99.61	99.22	99.34
Mg no.	20.6	19.4	26.6	4.0	8.2	13.6	16.9
Na_2O + K_2O	5.11	10.73	7.65	12.86	12.64	11.73	8.52
Trace elements	*ppm*	*ppm*	*ppm*	*ppm*	*ppm*	*ppm*	*ppm*
Cs	0.65	1.00	1.58	1.72	0.43	0.45	0.22
Rb	47.81	113.37	39.55	205.80	129.07	104.50	43.74
Ba	1179.05	1013.76	1165.20	21.31	614.40	1864.82	3150.79
Th	8.07	18.71	4.64	12.60	8.18	6.24	7.70
U	1.46	6.29	0.86	3.09	1.32	1.05	1.40
Ta	16.56	8.12	4.08	6.27	6.41	9.83	14.15
Nb	261.02	171.32	94.03	159.37	127.55	142.65	250.90
Mo	3.83	4.04	1.22	5.82	0.43	0.70	3.75
La	193.68	105.29	72.38	165.39	54.46	91.96	141.56
Ce	379.51	171.08	116.82	185.82	92.24	157.88	247.54
Sr	3938.04	1271.10	2242.44	25.36	329.52	747.45	3389.30
Nd	165.48	63.59	44.04	34.54	28.32	57.88	84.75
Hf	8.93	11.34	5.51	7.57	8.40	7.63	6.88
Zr	283.98	520.70	231.98	365.70	398.05	342.07	260.67
Y	66.09	29.37	20.14	13.37	17.33	27.60	36.21

Table 2. Continued.

Sample number	DL36	DL35	DJ43	DD25	DD26	DL33
Rock type	Bear-valley maifc syenite	Ghiduţ nepheline syenite	Ghiduţ nepheline syenite	Ghiduţ nepheline syenite	Ghiduţ nepheline syenite (altered)	Ghiduţ nepheline syenite
Majors	*wt. %*	*wt. %*	*wt. %*	*wt. %*	*wt. %*	*wt. %*
SiO_2	51.37	59.16	61.99	57.75	56.17	57.23
TiO_2	1.15	0.21	0.52	0.07	0.22	0.36
Al_2O_3	21.23	21.34	20.16	22.51	22.19	21.46
Fe_2O_3 TOTAL	5.17	2.08	1.69	2.24	1.57	2.48
Mn_3O_4	0.21	0.08	0.03	0.06	0.07	0.14
MgO	0.85	0.22	0.42	*0.05*	0.49	0.2
CaO	3.8	0.61	2.35	0.32	1.37	1.39
Na_2O	8.47	8.54	7.31	12.81	12.94	8.41
K_2O	4.65	6.29	4.18	2.55	0.72	6.1
P_2O_5	0.2	0.03	0.09	<0.01	<0.01	0.04
LOI	1.92	1.23	0.35	1.16	3.6	1.3
Total	99.5	99.83	99.85	99.67	99.89	99.2
Mg no.	12.4	8.4	17.6	1.9	21.2	6.5
Na_2O + K_2O	13.12	14.83	11.49	15.36	13.66	14.51
Trace elements	*ppm*	*ppm*	*ppm*	*ppm*	*ppm*	*ppm*
Cs	1.09	1.02	0.52	0.62	2.26	0.67
Rb	107.53	288.80	64.63	84.04	44.37	184.83
Ba	1878.02	194.39	2958.91	109.99	194.85	230.89
Th	21.60	5.99	5.97	72.45	3.48	4.49
U	2.58	1.75	1.40	33.80	3.08	0.87
Ta	9.15	0.73	3.73	19.71	0.69	2.44
Nb	264.92	17.60	74.82	609.99	46.41	81.54
Mo	1.43	0.45	0.61	0.71	1.98	0.61
La	113.26	17.63	50.93	32.22	27.22	43.07
Ce	180.94	22.12	76.58	71.00	36.28	64.19
Sr	1444.63	170.91	1568.96	98.82	1010.28	194.16
Nd	52.83	5.47	25.32	19.28	10.31	14.19
Hf	9.91	1.63	18.96	20.48	0.20	5.92
Zr	484.44	68.54	1310.23	961.90	2.59	295.23
Y	28.60	3.00	13.23	13.78	2.60	10.89

Table 2. Continued.

Sample number	DL09	DL11	DL19	DL21	DD24	DD46	DD45
Rock type	LANS	LANS	LANS	LANS	LANS (most enriched)	LANS	Hagota quartz syenite
Majors	*wt. %*	*wt. %*	*wt. %*	*wt. %*	*wt. %*	*wt. %*	*wt. %*
SiO_2	59.22	61.79	60.19	61.48	59.5	58.17	66.29
TiO_2	0.23	0.34	0.18	0.3	0.17	0.64	0.44
Al_2O_3	22.45	18.36	22.56	20.64	23.12	20	16.48
Fe_2O_3 TOTAL	2.91	2.33	1.32	2.64	1.7	3.07	2.49
Mn_3O_4	0.12	0.15	0.05	0.04	*0.01*	0.12	0.08
MgO	0.38	0.17	0.21	0.45	0.12	1.06	0.32
CaO	0.11	1.68	0.08	0.14	0.06	1.25	0.65
Na_2O	5.19	6.52	5.3	5.68	6.53	5.17	6.03
K_2O	7.48	6.47	7.64	7.34	5.75	6.81	5.75
P_2O_5	0.02	0.04	0.02	0.04	<0.01	0.06	0.06
LOI	1.27	1.34	1.45	1.09	1.92	2.43	0.38
Total	99.71	99.47	99.07	99.94	99.22	99.09	99.08
Mg no.	10.1	5.9	12.1	12.8	5.7	22.9	10.0
$Na_2O + K_2O$	12.67	12.99	12.94	13.02	12.28	11.98	11.78

Trace elements	*ppm*	*ppm*	*ppm*	*ppm*	*ppm*	*ppm*	*ppm*
Cs	0.59	0.93	0.31	0.59	0.38	4.45	1.34
Rb	278.54	160.49	272.78	227.46	254.54	224.68	215.56
Ba	518.97	585.37	227.88	378.84	211.93	1328.03	392.76
Th	52.09	19.44	8.51	12.89	11.69	25.50	27.34
U	7.67	3.42	1.49	7.12	12.42	4.38	4.87
Ta	5.77	4.19	3.27	8.44	3.33	4.59	8.79
Nb	302.27	115.95	85.74	200.01	306.54	154.20	137.28
Mo	0.28	0.12	0.26	0.42	11.69	1.20	0.52
La	22.61	64.59	25.24	41.06	23.41	105.64	53.34
Ce	28.56	86.11	35.91	72.74	22.35	120.06	99.25
Sr	306.82	342.90	131.11	273.95	25.81	765.26	154.60
Nd	7.23	20.03	9.80	20.20	3.14	32.80	36.11
Hf	22.10	14.14	5.33	4.79	22.42	7.98	10.99
Zr	1174.91	924.33	256.76	178.15	1593.87	448.65	472.15
Y	4.88	13.07	5.48	8.76	7.91	18.94	28.67

Throughout the Ditrău Complex Zr and SiO_2 show no significant correlation (Fig 8). This indicates that fractional crystallisation is not the main control on Zr content within the more evolved lithologies. The whole-rock Th/U ratio is typically >1.4 for unaltered magmatic lithologies; however, trace element concentrations in the Ghiduţ nepheline syenite are variable and the Th/U ratio ranges from 1.3 to 0.5 depending on sample locality. In primitive mantle normalised trace element plots (Fig 9(a)) the mafic lithologies show trace element patterns similar to Ocean Island Basalts (OIB), being enriched in high field strength elements (HFSE). The Jolotca amphibolite and Sărmaș Gabbro have the highest concentrations of Sr and high concentrations of Ta and Nb. The Ditrău syenite and Hagota quartz syenite have relatively high concentrations of Rb, K, Hf and Zr but are depleted in Ba and Sr. The Hagota quartz syenite also shows notable enrichment in Th and U compared to the more mafic lithologies.

Alteration of the nepheline syenite lithologies had a pronounced effect on their trace element concentrations (Fig 9(b)). The Ghiduţ nepheline syenite adjacent to a cross-cutting mafic dyke is extensively altered in comparison to the fresh Ghiduţ nepheline syenite and is depleted in the HFSE. The cross-cutting mafic dyke has a relatively flat trace element pattern with concentrations of the HFSE comparable to concentrations in the mafic lithologies.

The LANS shows clear enrichment in the HFSE likely corresponding to the presence of abundant large zoned zircons; this enrichment is further emphasised in the most mineralised LANS sample (Fig 9(b)). In particular, this sample shows a strong positive Nb anomaly, reflecting the amount of pyrochlore observed in hand specimens. The Th/U ratio decreases from 1.5 in the LANS to 0.2 in the most zircon-rich LANS samples. The LANS is typically depleted in Cs, Ba and Sr, with Sr concentrations in the most zircon-rich LANS <26 ppm.

All magmatic lithologies of the Ditrău Complex are relatively light rare earth element (LREE) enriched and have smooth patterns, typically lacking Eu anomalies (Fig 10; Table 3). However, the $(La/Lu)_N$ ratio varies widely from 13 for the Hagota quartz syenite to 34 for the Jolotca amphibolite. The mafic lithologies have the highest total REE values, reaching 871 ppm for the Jolotca amphibolite and 544 ppm for the Sărmaș Gabbro. Within these lithologies, the known REE-bearing phases are cumulus titanite and apatite and the lithologies with highest TiO_2 are also enriched in the REE, indicating titanite may play a role in magmatic REE enrichment. A cross-cutting mafic dyke in the Ghiduţ nepheline syenite shows a relative enrichment in REE compared to the syenites, with a similar pattern to the Jolotca amphibolite. The Hagota quartz syenite has the highest whole-rock concentrations of REE among the syenites and is the only lithology to show a minor negative Eu anomaly (Eu/Eu*=0.47), indicative of plagioclase fractionation and/or crustal contamination. Interestingly, the Ghiduţ nepheline syenites and the LANS show relatively low REE concentrations, but some samples have a weakly concave pattern, with higher normalised concentrations of the HREE. Higher concentrations of HREE in the LANS relative to the Ghiduţ nepheline syenite correlate with zircon abundance. The depletion of the middle rare earth elements (MREE) is most pronounced in samples of LANS and altered Ghiduţ nepheline syenite. These altered lithologies are also depleted in the LREE relative to the other syenitic lithologies.

The mineralised veins that cross-cut the intrusion were not analysed for whole rock geochemistry due to their small-scale heterogeneity. The mineralogy of the samples indicates that this lithology has the highest concentrations of REE, due to the prevalence of REE-bearing phases. Sabau (2015, pers. comm.) recognised two generations of monazite based on the thorium content: (1) an early phase of Th-poor monazite and, (2) a later (main) Th-rich monazite. From XRF analysis in the field and EDS SEM analysis of polished sections, only the Th-rich type was observed in the mineralised samples collected as part of this study.

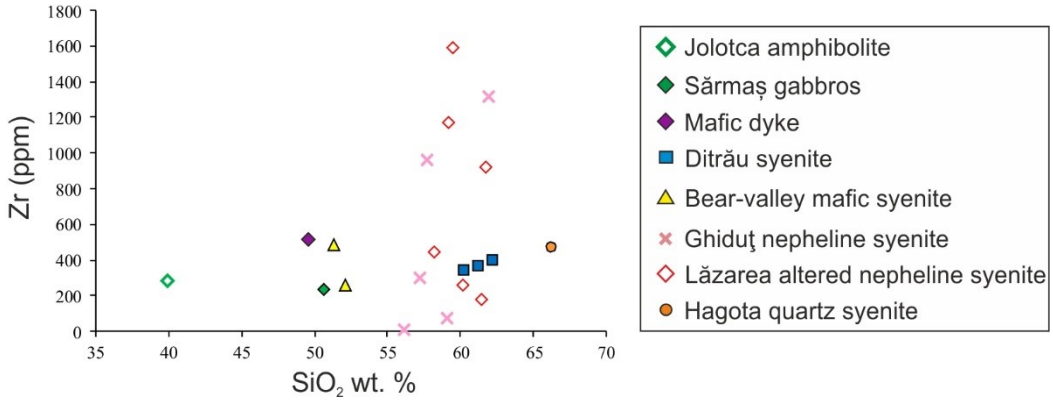

Figure 8. Plot of SiO2 wt. % against Zr (ppm) for the Ditrău complex.

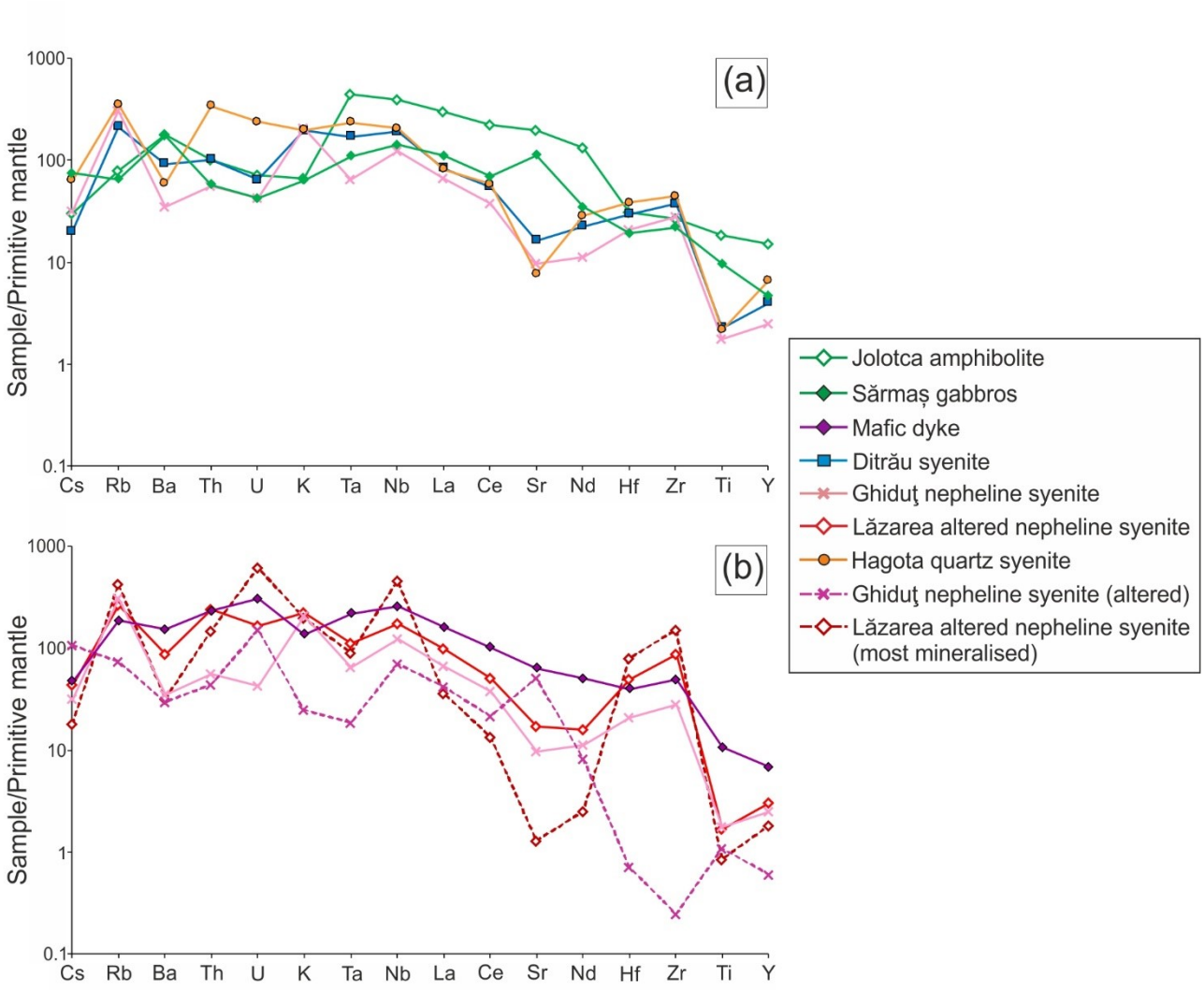

Figure 9. Primitive-mantle normalised spider diagram for representative samples of the different lithologies within the Ditrău alkaline complex. Normalising values from McDonough & Sun (1995). (a) Magmatic lithologies; (b) Altered lithologies with magmatic lithologies.

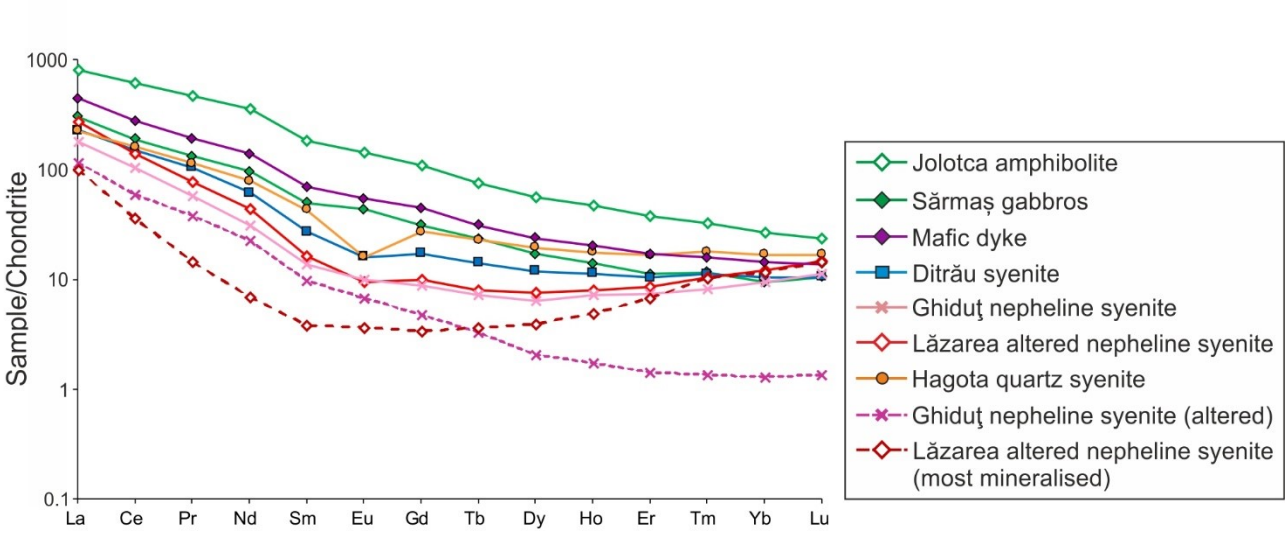

Figure 10. Chondrite normalised rare earth element diagram for samples of the different lithologies within the Ditrău alkaline complex. Normalising values from McDonough & Sun (1995).

Table 3. Whole rock REE element data. Lăzarea altered nepheline syenite is abbreviated to LANS.

Sample number	**DJ01**	**DL34**	**DD30**	**DD22**	**DL32**	**DJ44**	**DD29**
Rock type	Jolotca amphibolite	Mafic dyke (Sărmaș gabbro)	Deformed Sărmaș gabbro	Ditrău syenite	Ditrău syenite	Ditrău syenite	Bear-valley mafic syenite
REE	*ppm*	*ppm*	*ppm*	*ppm*	*ppm*	*ppm*	*ppm*
La	193.68	105.29	72.38	165.39	54.46	91.96	141.56
Ce	379.51	171.08	116.82	185.82	92.24	157.88	247.54
Pr	44.13	17.83	12.30	13.78	9.75	16.86	25.70
Nd	165.48	63.59	44.04	34.54	28.32	57.88	84.75
Sm	27.01	10.34	7.42	3.83	4.07	9.15	13.60
Eu	8.18	3.09	2.47	0.64	0.90	2.42	4.00
Gd	21.67	8.89	6.21	2.69	3.47	7.13	10.26
Tb	2.74	1.13	0.86	0.39	0.51	0.98	1.38
Dy	14.02	5.87	4.20	2.23	2.94	5.16	7.45
Ho	2.58	1.11	0.77	0.48	0.62	1.04	1.36
Er	6.03	2.76	1.81	1.37	1.68	2.61	3.43
Tm	0.82	0.39	0.29	0.24	0.28	0.39	0.47
Yb	4.31	2.32	1.53	1.66	1.70	2.14	2.62
Lu	0.59	0.34	0.26	0.31	0.26	0.30	0.36
REE_{TOTAL}	870.75	394.02	271.35	413.37	201.21	355.88	544.49
$(La/Lu)_N$	10	86	25	14	55	22	16

Table 3. Continued.

Sample number	**DL36**	**DL35**	**DJ43**	**DD25**	**DD26**	**DL33**	**DL09**
Rock type	Bear-valley maifc syenite	Ghiduţ nepheline syenite	Ghiduţ nepheline syenite	Ghiduţ nepheline syenite	Ghiduţ nepheline syenite (altered)	Ghiduţ nepheline syenite	LANS
REE	*ppm*	*ppm*	*ppm*	*ppm*	*ppm*	*ppm*	*ppm*
La	113.26	17.63	50.93	32.22	27.22	43.07	22.61
Ce	180.94	22.12	76.58	71.00	36.28	64.19	28.56
Pr	17.12	1.87	7.57	6.55	3.52	5.41	2.57
Nd	52.83	5.47	25.32	19.28	10.31	14.19	7.23
Sm	7.65	0.78	3.81	2.60	1.45	2.03	1.09
Eu	2.41	0.25	1.37	0.71	0.38	0.56	0.28
Gd	6.16	0.65	3.17	2.13	0.95	1.77	0.83
Tb	0.91	0.10	0.44	0.34	0.12	0.26	0.13
Dy	4.94	0.52	2.44	2.11	0.51	1.58	0.77
Ho	1.03	0.12	0.47	0.51	0.10	0.40	0.20
Er	2.73	0.31	1.32	1.58	0.23	1.19	0.59
Tm	0.44	0.06	0.20	0.30	0.03	0.20	0.12
Yb	2.65	0.37	1.31	1.88	0.21	1.54	0.89
Lu	0.40	0.07	0.22	0.33	0.03	0.28	0.17
REE_{TOTAL}	393.47	50.34	175.15	141.56	81.33	136.69	66.06
$(La/Lu)_N$	32	18	22	31	7	24	40

Table 3. Continued.

Sample number	DL11	DL19	DL21	DD24	DD46	DD45
Rock type	LANS	LANS	LANS	LANS (most enriched)	LANS	Hagota quartz syenite
REE	*ppm*	*ppm*	*ppm*	*ppm*	*ppm*	*ppm*
La	64.59	25.24	41.06	23.41	105.64	53.34
Ce	86.11	35.91	72.74	22.35	120.06	99.25
Pr	7.17	3.49	6.87	1.33	11.54	10.71
Nd	20.03	9.80	20.20	3.14	32.80	36.11
Sm	2.45	1.45	2.81	0.56	4.15	6.42
Eu	0.53	0.29	0.53	0.21	1.22	0.91
Gd	2.01	1.16	2.32	0.67	3.19	5.42
Tb	0.29	0.17	0.32	0.13	0.44	0.83
Dy	1.86	0.95	1.79	0.97	2.57	4.83
Ho	0.44	0.21	0.35	0.27	0.57	0.98
Er	1.38	0.62	0.99	1.09	1.71	2.68
Tm	0.26	0.11	0.14	0.25	0.29	0.45
Yb	1.97	0.74	0.89	1.85	1.90	2.73
Lu	0.37	0.12	0.14	0.36	0.28	0.42
REE_{TOTAL}	189.47	80.27	151.14	56.60	286.36	225.08
$(La/Lu)_N$	29	34	41	29	32	13

Apatite mineral chemistry

Apatite grains from eight different rock types and vein systems throughout the complex were analysed by EPMA, to investigate variations in REE concentration; six of the samples contain apatite with total REE >1 wt.%. The analysed samples are representative of the Jolotca amphibolite; the LANS; and the mineralised veins in the Jolotca region, abbreviations used are detailed in Table 4. The LANS is extensively cross-cut by aplite, biotite and carbonate veins; apatite crystals from these veins were analysed. Data for these samples are presented in Supplementary Table 2.

Apatite volatile contents

The F content of Ditrău apatites varies between 2.30 and 4.92 wt. %, while the Cl content is typically below 0.32 wt. %. Samples collected during this study from the Ditrău Complex contain no chlorapatite (based on apatite data collected); this is in agreement with observations by Piccoli and Candella (2002) that chlorapatite is generally rare. Stoichiometric fluorapatite can contain a maximum of 3.76 wt. % F (Pyle et al., 2002); therefore the apatite crystals from this study with F concentrations >3.76 wt. % are classified as end-member fluorapatite within analytical uncertainty, as the excess F is likely due to F migration under the electron beam (Stock et al., 2015). The LANS, and the cross-cutting veins within it, are dominated by end-member fluorapatite.

Jolotca amphibolite

The apatite within the Jolotca amphibolite (Ap_{JA}) has the highest Cl concentration relative to the other apatites, with a maximum Cl value of 0.32 ± 0.06 wt. %. Ap_{JA} have the lowest total REE (TREE + Y) content of all apatites analysed, with a maximum Ce value of 0.27 wt. % ± 0.02, and an average of 0.10 wt. %. The maximum Y value is 0.03 ± 0.02 wt. %. All apatite REE patterns for this lithology are similar, whether as inclusions in titanite, biotite or amphibole. The REE pattern of Ap_{JA} shows a distinct enrichment in LREE, decreasing linearly with a shallow gradient to Y (Fig 11(a)), as is typical of magmatic apatite analysed in layered intrusions (e.g. Rønsbo, 2008; VanTongeren and Mathez, 2012).

Lăzarea altered nepheline syenite (LANS)

Apatites within the LANS are LREE-enriched with low Y concentrations, forming a linear pattern (Fig 11 (b, c)). Ap_{LANS} crystallised within the body of the LANS and has a Ce maximum concentration of 2.28 ± 0.04 wt. %, La a maximum of 1.41 ± 0.04 wt. % and Y a maximum of 0.84 ± 0.02 wt. %. Apatites adjacent to biotite typically have lower concentrations of REE, but only a limited number of biotite-adjacent apatites were analysed. Apatites from the margins of the LANS typically have lower TREE + Y contents (Supplementary Table 2).

Aplitic syenite vein cutting the LANS

The aplite vein apatite (Ap_{APLITE}) is the most LREE-enriched in the complex (Fig 11(d)). Ap_{APLITE} TREE + Y element values range from 1.18 to 7.01 wt. %. Ce is the dominant REE with an average concentration of 1.83 wt. % and a maximum of 3.39 ± 0.06 wt. %, followed by La with an average of 1.21 wt. % and maximum of 2.37 ± 0.06 wt. %. Nd has a maximum concentration of 0.74 ± 0.06 wt. %, whilst Y has an average concentration of 0.23 wt. % and a maximum of 0.38 ± 0.02 wt. %; this forms the typical Ditrău REE pattern with a downward linear slope. There is variability in the TREE + Y concentrations of Ap_{APLITE}, but there is no obvious correlation between the apatite position within the vein and the REE content.

Biotite-rich vein cutting the LANS

The apatite in the biotite-rich vein (Ap_{BV}) is LREE dominated with low TREE + Y concentration variability (Fig 11(e)). Only apatite grains from the centre of the vein were large enough for EPMA. The maximum La concentration is 0.40 ± 0.02 wt. % with an average of 0.27 wt. %. The average Nd and Y concentrations are 0.14 wt. % and 0.07 wt. % respectively forming a linear LREE-enriched pattern.

Carbonate veins cutting the LANS

The apatites within the carbonate vein cutting the LANS are LREE-dominated, forming two distinct apatite populations of: (1) small REE-enriched apatites, $Ap_{CV(S)}$ and (2) large REE-depleted apatites $Ap_{CV(L)}$ (Fig 11(f)). The Ce range in the REE-enriched group is 1.92 ± 0.04 to 2.59 ± 0.06 wt. % and 0.64 ± 0.04 to 1.07 ± 0.04 wt. % in the REE-depleted group. The maximum value for Y within the REE-enriched group is 0.25 ± 0.02 wt. % whilst in the REE-depleted group it is 0.12 ± 0.02 wt. %. The REE pattern is a linear declining trend, from high LREE to low Y; this pattern is the same for both apatite groups. A number of apatites within the carbonate vein have altered rims, which typically show slightly more enrichment in REE + Y than the apatite cores. This correlates with higher Na_2O and SiO_2 and lower CaO concentrations. Compositional profiles across unaltered apatite grains have relatively flat REE profiles suggesting a low degree of magmatic geochemical zonation in these grains.

Mineralised veins cutting the Sărmaș gabbro and Jolotca amphibolite

Within the mineralised veins there are three distinct populations of apatite: (1) apatite inclusions in, or along the margins of allanite (Ap_{ALN}; Fig 11(g)); (2) apatite trapped as inclusions within pyrite grains (Ap_{PY}; Fig 11(h)); and (3) apatite hosted in carbonate gangue (Ap_{MV}; Fig 11(h)).

The shape of the REE patterns from all three apatite grain populations in the mineralised vein is distinctly different to that of apatites in the other lithologies of the Ditrău Complex. The pattern is typically a flattened

convex shape with a curved increase from La to Nd, then a plateau or small decrease to Y, and contrasts with the linear LREE enriched patterns seen in the other lithologies.

The apatites within the mineralised veins have very high TREE + Y concentrations, with the apatite inclusions hosted in pyrite (Ap_{PY}) reaching TREE + Y values of 7.09 wt. %. La has an average concentration of 0.52 wt. % with a maximum of 1.03 ± 0.08 wt. %, whilst Nd has an average of 1.53 wt. %, with a maximum of 1.94 ± 0.16 wt. %. Y has a maximum value of 2.12 ± 0.10 wt. %. Ce has the highest concentration at 3.03 ± 0.10 wt. %. From the pyrite core to the rim, apatite inclusions show decreasing LREE contents and increasing HREE contents. The apatite grains with the lowest La and Ce have the highest Nd and Y concentrations, whilst those with the highest La and Ce concentrations have only mid-range Nd and Y concentrations.

The pyrite grains are commonly fractured and apatite inclusions lying adjacent to these fractures have alteration rims, identifiable in BSE. These rims are depleted in REE; La and Ce are preferentially depleted compared to Y. This depletion is at odds with the enrichment trends seen in apatite alteration rims within carbonate veins in the LANS (Ap_{CV}).

The Ap_{PY} contains two geochemically distinct populations of inclusions. These were identified using SEM-EDS point analysis, one population is enriched in LREE (monazite) and the other is enriched in HREE (xenotime).

The carbonate gangue hosted apatites (Ap_{MV}) have the lowest TREE + Y concentrations of the three apatite populations within the mineralised veins, averaging <1 wt. % (Supplementary Table 2). Average La and Ce concentrations of Ap_{MV} are markedly low. The apatites associated with allanite (Ap_{ALN}) have TREE + Y concentrations averaging 0.24 wt. %, with average La concentrations of 0.03 wt. %, average Nd concentrations of 0.05 wt. %, and an average Y value of 0.06 wt. %.

Strontium concentrations also distinguish the apatite grains of the mineralised veins from the apatite grains analysed in other lithologies. In the LANS, apatite grain SrO concentration is typically below detection limit. However, in the mineralised veins the carbonate gangue hosted apatite grains (Ap_{MV}) have an average SrO concentration of 3.07 wt. %, with a maximum of 4.39 ± 0.40 wt. %. The apatite inclusions in pyrite (Ap_{PY}) have an average of 1.73 wt. % SrO, with a maximum of 3.71 ± 0.36 wt. % for an apatite inclusion from the pyrite rim. Excluding the pyrite rim apatites, the maximum SrO value is 2.32 ± 0.30 wt. %. Apatite associated with allanite (Ap_{ALN}) has lower SrO values with an average concentration of 0.34 wt. % and a maximum of 0.90 ± 0.05 wt. %.

REE substitution mechanisms into apatite

The LREE enrichment in apatites from the LANS (Ap_{LANS}, Ap_{BV}, Ap_{CV} and Ap_{ALN}) is accompanied by a positive correlation between the concentration of REE and SiO_2 in the apatite, negative correlation between REE and P_2O_5 and no correlation between REE and Na_2O. The calculated Si, P and Na cation content shows that the REE enrichment is due to the substitution: $REE^{3+} + SiO_4^{4-} = Ca^{2+} + PO_4^{3-}$ (Fleet & Pan, 1995; Pan & Fleet, 2002; Ronsbo, 1989; Fig 12). Other charge-compensating mechanisms can be used for the substitution of Ca^{2+} by REE^{3+}. Potentially the mechanism: $2REE^{3+}$ + vacancy = $3Ca^{2+}$ (Pan and Fleet, 2002) could be responsible for the substitution of REE into apatite in the Ditrău Complex, but this is not supported by our data.

The low Si and elevated Na concentrations in Ap_{PY} and Ap_{MV} hosted by the mineralised veins indicate that a different mechanism may control the substitution of REE into these apatites (Fig 12). Since Na correlates with the REE, the substitution mechanism is likely to be: $REE^{3+} + Na^{+} = 2Ca^{2+}$ for these lithologies (Pan & Fleet, 2002). Apatites within the LANS show different REE substitution mechanisms; apatites closer to the intrusion margin (sample DD23) are aligned with the mineralised veins (Fig 12).

Within the Ap_{JA} the calculated Na and Si cation content shows that the REE enrichment is balanced by a contribution from two substitutions: $REE^{3+} + Na^{+} = 2Ca^{2+}$ and $REE^{3+} + SiO_4^{4-} = Ca^{2+} + PO_4^{3-}$ (Pan & Fleet, 2002; Fig 12).

Apatite grains in the centre of the LANS, including those in the carbonate veins, show distinctly different REE patterns and substitution mechanisms when compared with the apatite in the mineralised veins. This indicates that the mineralised veins in the Jolotca area are derived from a distinctly different source to the fluids involved in alteration of the LANS.

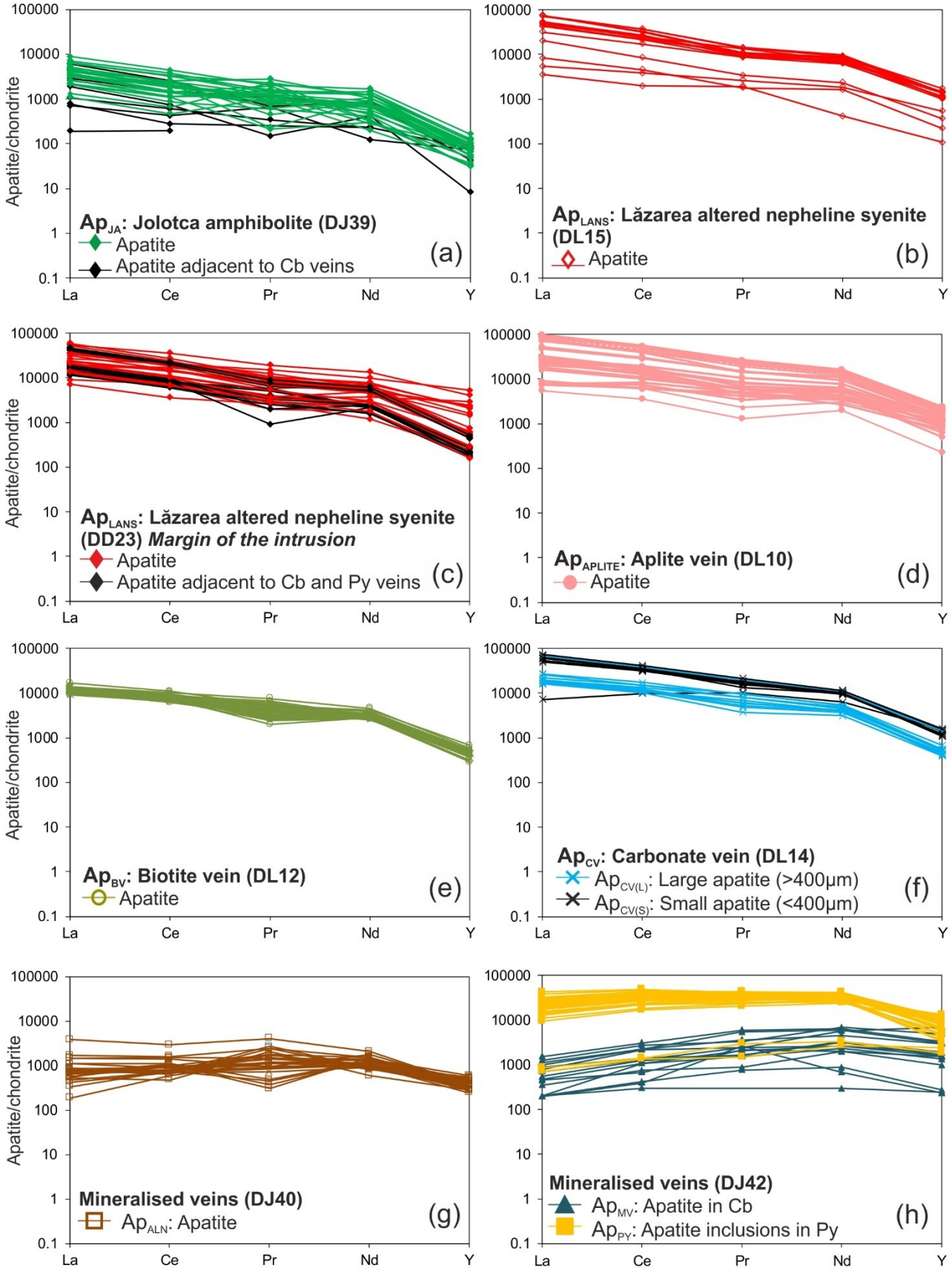

Figure 11. Chondrite-normalised apatite REE concentrations for La, Ce, Pr, Nd and Y, after McDonough & Sun (1995). Black symbols and lines are used to show anomalous textural groupings of apatite or different size groupings, as detailed on the graphs. (a) Jolotca amphibolite, DJ39; (b) Lăzarea altered nepheline syenite, DL15; (c) Lăzarea altered nepheline syenite, DD23; (d) Aplite vein, DL10; (e) Biotite-rich vein, DL12; (f) Carbonate vein, DL14; (g) Mineralised vein, DJ40; (h) Mineralised vein, DJ42.

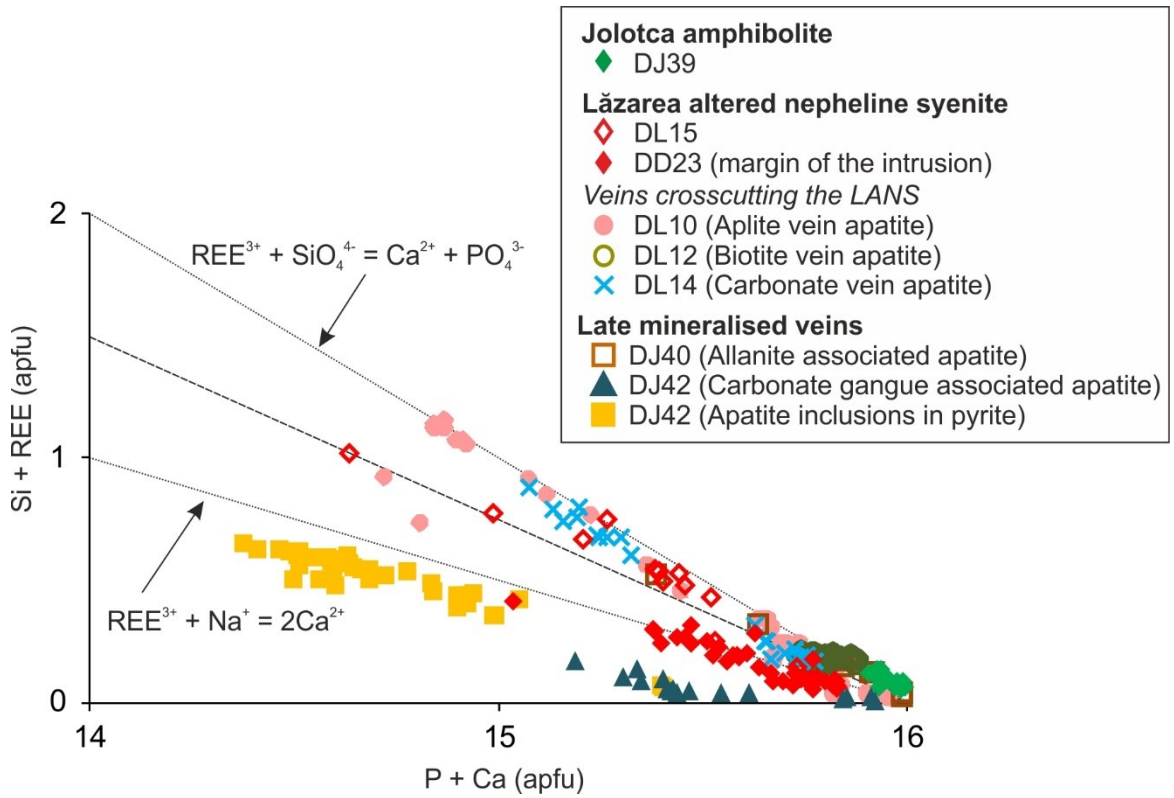

Figure 12. Substitution of REEs into apatite from the Ditrău Complex. The dashed line represents an equal contribution from the two substitutions: $REE^{3+} + SiO4^{4-} = Ca^{2+} + PO4^{3-}$ and $REE^{3+} + Na^{+} = 2Ca^{2+}$, lines plotted as of Pan and Fleet, (2002).

Table 4. A summary of lithologies from which apatites were analysed. The apatite mineral chemistry is referred to through the apatite abbreviation.

Lithology	Sample number	Apatite Abbreviation
Jolotca amphibolite	DJ39	Ap_{JA}
Lăzarea altered nepheline syenite (LANS)	DL15	Ap_{LANS}
Lăzarea altered nepheline syenite (LANS)	DD23	Ap_{LANS}
Aplite vein cutting LANS	DL10	Ap_{APLITE}
Biotite vein cutting LANS	DL12	Ap_{BV}
Carbonate vein cutting LANS	DL14	
Large apatites		$Ap_{CV(L)}$
Small apatites		$Ap_{CV(S)}$
Mineralised vein apatite		
Apatite adjacent to allanite	DJ40	Ap_{ALN}
Apatite hosted in the carbonate gangue	DJ42	Ap_{MV}
Apatite inclusions in large pyrite grains	DJ42	Ap_{PY}

DISCUSSION

The Ditrău Complex, and extensive associated mineralisation, has formed by the interplay of magmatic and hydrothermal processes. The initial architecture of the magma chamber developed through magmatic processes such as fractional crystallisation and crystal settling. As the magma chamber cooled, there was extensive hydrothermal alteration of the magmatic rocks which is considered to be attributable to late-stage magmatic fluids, and may have overlapped with the final stages of magmatism. Finally, late mineralised veins represent the later stages of the hydrothermal system. These processes are discussed below in turn.

Magmatic processes

Formation of ultramafic cumulates

Previous work on the Ditrău Complex has suggested a number of different models for the nature of the magma chamber. Here, we propose a model of a layered magma chamber (Fig 13) that has been tilted subsequent to emplacement. The petrologic and whole-rock geochemical data for virtually all the Ditrău magmatic lithologies are consistent with evolution by fractional crystallisation of an alkaline parental magma, with the Jolotca amphibolite representing ultramafic cumulates. These ultramafic cumulates are amphibole-dominated with extensive titanite and apatite, implying a relatively volatile-rich magma (Fall et al., 2007). The ultramafic cumulates lack an Eu anomaly and cumulus apatite has high Sr concentrations, implying that plagioclase fractionation was not an important process at Ditrău. The ultramafic cumulates have the highest whole rock REE concentration among the magmatic lithologies at Ditrău, and are also enriched in Ta, Nb and Ti relative to the other magmatic rocks. Cumulate titanite is modally significant in these rocks and the high partition coefficients of HFSE into titanite make it an important host (Tiepolo et al., 2002). The Ta–Nb ratio is higher in the ultramafic cumulates than in the gabbroic and syenitic rocks, due to Ta preferentially partitioning into titanite over Nb.

The enriched REE patterns for the ultramafic cumulates are similar to those of Mount Erebus (Kyle et al., 1992); there the pattern was attributed to the accumulation of apatite, titanite and kaersutite. In the early crystallising magmas of the Ditrău Complex, the REE behaved compatibly and were incorporated into cumulus minerals such as titanite and apatite. This indicates early REE saturation in the magma, with the REE removed from the melt before the more evolved lithologies crystallise; similar early crystallisation of REE-bearing minerals is also observed in the Loch Loyal Syenite Complex in the UK (Walters et al., 2013).

Enrichment in evolved magmas

Amphibole and titanite fractionation from the Ditrău parental magmas has led to the formation of more evolved, silica-undersaturated magmas which crystallised as syenites and nepheline syenites with low concentrations of Mg, Ti, Fe and Ca. Total alkalis are high throughout the crystallisation sequence, and an inflection in Al_2O_3 and Na_2O contents at c. 55 wt. % SiO_2 marks the onset of alkali feldspar fractionation and nepheline accumulation.

Notably, the early crystallisation of titanite and apatite means that REE and HFSE contents are relatively low in the fresh Ghiduţ nepheline syenites. These nepheline syenites have a weak concave REE pattern, and lack an Eu anomaly. Eby et al., (1998) stated that such a pattern in magmatic rocks may potentially form by titanite fractionation or zircon accumulation.

The MREE have higher partition coefficients for titanite than either LREE or HREE (Green and Pearson, 1987; Tiepolo et al., 2002). At Ditrău, titanite reached the liquidus early in the crystallisation history, depleting the residual melt in MREE.

The HREE have a high partition coefficient for zircon relative to LREE (Fujimaki, 1986; Thomas et al., 2002), therefore accumulation of zircon would lead to an enrichment of the rock in HREE. Petrogenetic evidence supports zircon accumulation within the Ghiduţ nepheline syenite, reflecting the miaskitic and alkaline nature of the Ditrău Complex (Sheard et al., 2012). Two generations of zircon are recognised: inclusion-rich zircon and compositionally homogenous zircon (often with a rim of inclusion-rich zircon). The homogenous zircon

crystallised deeper in the magma chamber, when zircon first reached the liquidus. The inclusion-rich zircon crystallised in-situ in the more evolved lithologies, as the inclusions are continuous with the surrounding matrix.

The accumulation of magmatic zircon contributes towards the relatively high Hf, Zr, U and Th concentrations in the Ghiduţ nepheline syenite, which is also enriched in Nb relative to Ta. High Nb/Ta ratios in the nepheline syenites can largely be related to the fractionation of titanite from the evolving magma (Marks et al., 2008) as Ta preferentially partitions into titanite (Green and Pearson, 1987).

Fall et al., (2007) studied fluid inclusions from the Ghiduţ nepheline syenite and identified a co-existing high salinity, carbonate-rich aqueous fluid with 20–40 wt. % NaCl which was interpreted as having exsolved from the melt during crystallisation, such that an active magmatic hydrothermal system existed during much of the crystallisation history. The relatively high Cl content in the Jolotca amphibolite apatites provides an indication that this magmatic hydrothermal system developed after the ultramafic cumulates were formed.

The most extensive magmatic-hydrothermal alteration occurred in the LANS, and therefore only limited information about magmatic processes can be gleaned from this unit, which is interpreted as having originally been a roof-zone nepheline syenite somewhat less evolved than the Ghiduţ nepheline syenite. However, the apatites within the LANS are considered to represent part of the magmatic history.

Apatite modal abundance in the LANS is lower than in the Ditrău syenite, indicating the melt had continued fractionating towards apatite-out. Apatite shapes are acicular, typical of disequilibrium crystallisation and rapid cooling (Webster and Piccoli, 2015). From textural relations, fluorapatite is a magmatic phase. Ap_{LANS} has the same magmatic REE pattern as the Ap_{JA}, but with greater REE concentrations; such patterns are common in nepheline syenites such as the Pilanesberg Alkaline Complex in South Africa (Liferovich and Mitchell, 2006). Experimental work and data from natural assemblages have shown that REE uptake in natural apatite is highest for MREE and lowest for LREE and HREE, forming a convex pattern (Fleet and Pan, 1997; Rønsbo, 2008; Watson and Green, 1981). Therefore, convex shaped REE patterns would be expected of apatite mineralogy data, if conditions were constant and the REEs all had the same concentration in the parental melt: this is not the case in the magmatic lithologies of the Ditrău Complex, therefore this indicates an LREE-enriched parental melt.

The differing coupled substitution mechanisms observed in apatite throughout the complex are interesting, especially the variation in the LANS apatite grains, which appears to be related to position in the intrusion. A key control on REE partitioning into apatite is the melt composition during apatite crystallisation, which is affected by the phases contemporaneously crystallising with apatite. Overall, REE contents in the melt increase with degree of fractionation within the complex (Larsen, 1979), because as the degree of polymerization increases there is a decrease in the number of melt sites suitable for REE^{3+} (Pan and Fleet, 2002). Consequently, Ap_{LANS} has high LREE concentrations (La+Ce up to 5.5 wt. %). The Si-coupled substitution reaction is dominant in magmatic apatite in the Ditrău Complex; as the magma fractionated, melt Si concentration would increase, causing increased polymerisation. Fewer melt sites would be suitable for REE and the high Si content would have promoted the coupled substitution: $Ca^{2+} + P^{5+} = REE^{3+} + Si^{4+}$ (Pan and Fleet, 2002). Silica will not buffer this coupled substitution as the melt is evolved, therefore the apatite REE record is assumed to reflect that of the melt, for these samples. Apatite near the intrusion margin in the LANS (sample DD23) has a different substitution mechanism to the other LANS apatites. The LANS marginal sample was sampled from the roof zone immediately adjacent to the country rock. These samples were uniquely associated with fluorite, consequently the magma chamber conditions near the margins could have caused the substitution reaction to change.

The Hagota quartz syenite is silica-saturated and thus diverges from the nepheline syenite fractionation trend and Na_2O Harker plot trend. It is not possible for nepheline syenite and quartz syenite to evolve from the same magma by fractional crystallisation alone (Gill, 2010), and so extrinsic factors are required for magma differentiation to produce a silica-saturated melt. The most likely explanation for this is crustal assimilation.

Morogan et al., (2000) measured $\delta^{18}O$ for quartz syenite, with values of 6.1 and 7.7 (% V-SMOW). These were higher relative to the rest of the Ditrău Complex, indicating that crustal assimilation played a role in the melt. The Hagota quartz syenite is characterised by a pronounced negative Eu and Sr anomaly, with a weaker Ba anomaly. This would typically be interpreted as a result of fractional crystallisation of plagioclase feldspar during melt genesis (Drake and Weill, 1975), as hypothesised by Morogan et al., (2000), but there is no evidence of substantial plagioclase fractionation within the Ditrău Complex and thus we consider this to represent crustal assimilation at the margins of the magma chamber. Siliceous country rock contamination occurred relatively early in evolution of the Ditrău Complex, at the margins of the evolving magma chamber, with minimal contamination affecting evolved melts in the core of the chamber later in the crystallisation history (Morogan et al., 2000).

Magmatic-hydrothermal processes

As discussed above, a magmatic-hydrothermal system is considered to have developed in the latter stages of crystallisation of the Ditrău Complex, and is evident firstly in progressive alteration of the Ghiduţ nepheline syenite, and subsequently in the highly altered nature of the LANS.

Sodic alteration

The earliest stages of this alteration are apparent in the Ghiduţ nepheline syenite, which has extensive cancrinite development along nepheline grain boundaries. Nepheline breaks down to cancrinite with the addition of (1) calcium carbonate, or (2) a complex carbonate:

(1) $6\ NaAlSiO_4 + 1.5\ CaCO_3 + 1.1\ H_2O = Na_6Ca_{1.5}(AlSiO_4)_6(CO_3)_{1.5}\ \ 1.1\ H_2O$
has been experimentally determined at 750–1000 °C (Edgar, 1964; Sirbescu and Jenkins, 1999).

(2) $6\ NaAlSiO_4 + 2\ Ca(Cl_2, CO_3, SO_4) + H_2O = Na_6Ca_{1.5}(AlSiO_4)_6(Cl_2, CO_3, SO_4)_2\ \ 1.1\ H_2O$
forming at 400–500 °C (Fall et al., 2007).

Small veins of calcite cut the Ghiduţ nepheline syenite, indicating the presence of a late-stage carbonate fluid, which promoted alteration from nepheline to cancrinite by a nepheline-carbonate reaction. Nepheline grains have typically not been fully replaced by cancrinite, therefore the reaction was buffered by the volume of the fluid or the concentration of carbonate in the fluid.

The Ghiduţ nepheline syenite is also characterised by rarer occurrences of interstitial sodalite along nepheline grain boundaries; this is a high temperature, low pressure phase in which chlorine is an essential component (Sharp and Helffrich, 1989a). It is common in hydrothermally altered igneous rocks but can be a primary phase in alkali layered intrusions (Deer et al., 1992; Eby et al., 1998; Finch, 1991; Sørensen and Larsen, 1987). It forms hydrothermally through the reaction:

$6\ NaAlSiO_4 + 2\ NaCl = Na_8Al_6Si_6O_{24}Cl_2$ (Finch, 1991; Sharp and Helffrich, 1989b).

Fall et al., (2007) reported a high-salinity fluid present whilst the Ghiduţ nepheline syenite was crystallising, with a lower salinity fluid trapped as fluid inclusions in cancrinite. This decrease in salinity is interpreted as indicating the uptake of Na and Cl from the fluid into cancrinite and sodalite during the early alteration of the nepheline syenites (Fall et al., 2007).

Albitisation would also have taken up Na; although this is not pervasive through the Ditrău Complex, recrystallised albite occurs in restricted patches in the Ghiduţ nepheline syenite, indicating that a Na-rich fluid flushed through (Hövelmann et al., 2010). Breakdown of Na-amphiboles (arfvedsonite) has led to the formation of a well-defined albite reaction rim hosting magnetite and pyrochlore; crystallisation of magnetite and pyrochlore requires additional Fe and Nb cations to be present in the fluid. Overall, all the data indicate that the earliest stages of alteration, evident in the Ghiduţ nepheline syenite, were due to a NaCl-rich fluid exsolved from the evolving alkaline magma, as proposed by Fall et al. (2007). This fluid may have been relatively rich in Nb, but did not produce any significant critical metal mineralisation.

Potassic alteration – fluid pathways

The second type of alteration recognised in the Ghiduţ nepheline syenite is associated with the mafic dykes that cut the lithologies of the Ditrău Complex. These dykes are typically altered to biotite, or have significant development of biotite along their margins. The unaltered mafic dyke contains amphibole. Biotitisation of hornblende is known to follow the generalised reaction:

hornblende + K_2SO_4 + H_2SO_4 = biotite + anhydrite + quartz
from experimental work (Brimhall et al., 1985; Speer, 1987).

Alteration of hornblende by a K-rich fluid is considered as the main process causing biotitisation of the mafic dykes. We suggest that the margins of the dykes represent pathways for K-rich fluids percolating through the Ditrău Complex, and it was this fluid, which caused the biotitisation of the mafic dykes. The analysed mafic dyke sample is notably more K-rich than other mafic lithologies (Fig 9).

The mafic dykes have a 1–2 m alteration zone in the surrounding Ghiduţ nepheline syenite. This zone is characterised by perthite, alteration of nepheline to micaceous aggregates, and biotite replacing amphibole. This mineral assemblage is characteristic of alteration by potassic fluids.

Crucially, the alteration halo is depleted in the REE and HFSE (Zr, Hf, Y, Ta and Nb) relative to unaltered Ghiduţ nepheline syenite (Fig 9); the U/Th ratio is similar to the mafic dyke's U/Th ratio, yet altered and unaltered lithologies are comparable in the concentration of LFSE. This is unexpected, as HFSE are commonly regarded as immobile, hence their use as indicators of evolution in geological systems (Gill, 2010; Pearce and Cann, 1973). However, recent observations and experimental work show that Zr, REE, Y, Nb, Th and U can be mobilised in alkali and F-rich systems (Ayers et al., 2012; Bernini et al., 2013; McCreath et al., 2012; Sheard et al., 2012; Wilke et al., 2013; Williams-Jones et al., 2012; Yang et al., 2014). Sheard et al., (2012) suggest in the Thor Lake deposit that LREE were transported as fluoride complexes in magmatic-hydrothermal fluids and that mixing with external, carbonate-rich, meteoric fluids caused fluorite and REE-carbonate deposition. In contrast, Williams-Jones et al. (2012) showed that chloride complexes are successful at mobilising the REE, but fluoride may be associated with their deposition.

The depletion of Zr and Hf suggests removal of zircon from the Ghiduţ nepheline syenite by fluid using the mafic dyke as a pathway. Notably, no zircon has been observed from petrologic study of the mafic dyke alteration halo, despite the abundance of zircon elsewhere in the Ghiduţ nepheline syenite. Geisler et al., (2001) undertook hydrothermal experiments on zircon at 450 ºC and 1.3 kbar; this produced zircon reaction rims depleted in Pb, Zr, Si and Th, whereas U remained in the structure. Dissolved ions within an aqueous fluid can have a significant effect on leaching kinetics of HFSE (Geisler et al., 2001). The experimental conditions are comparable to those inferred for the Ditrău Complex (Fall et al., 2007). If the zircon lattice was damaged by alpha-decay, the zircon would be more susceptible to alteration (Geisler et al., 2001; Geisler and Schleicher, 2000; Silver and Deutsch, 1963; Sinha et al., 1992), this is a possibility for the Ghiduţ nepheline syenite zircons, despite no radiation halos being observed in the petrogenic study. Alternatively, the inclusion-rich zones of the zircon may be more vulnerable to breakdown in the presence of a fluid.

Overall, a K-rich fluid has clearly used the mafic dykes as channels to rise upwards through the complex. This fluid, likely to have been rich in ligands such as F and Cl, had a leaching effect on the surrounding rocks, sequestering HFSE by the partial leaching of zircon. The origin of this fluid is not clear, although it should be noted that K-rich fluid alteration haloes are a common feature associated with carbonatites.

Potassic alteration in the roof zone

The LANS is considered to represent the roof zone of the Ditrău Complex and shows pervasive alteration of nepheline to micaceous aggregates, with no cancrinite. The LANS has the highest K_2O and high Al_2O_3 whole rock concentrations, but low CaO and Na_2O concentrations (Fig 5). Replacement of nepheline by micaceous aggregates is reported in the literature, with the alteration fluid inferred to be K-rich, and the alteration of

nepheline to micaceous aggregates known to release Na (Deer et al., 1992; Rimsaite, 1975). It is very likely that the Na released during nepheline alteration was removed by fluids and is now in the country rocks (fenites).

Zircon, titanite and pyrochlore occur in the LANS as rare magmatic phases, but are much more commonly associated with the K-rich alteration. In the LANS, fracture infills up to 1 mm in width concentrate HFSE-bearing and some REE-bearing minerals, e.g. zircon, pyrochlore and some monazite, bastnäsite, and allanite. It seems that K-rich fluids were transported through the complex, using the cross-cutting mafic dykes as pathways, and leaching the REE and HFSE from the surrounding syenites as they rose towards the roof zone. The increased fluid pressure on the solidified roof zone resulted in multiple micro-fractures, which are pervasive in the LANS. As the rock fractured, the decrease in pressure led to crystallisation of hydrothermal mineral assemblages along fractures. The fluid that accumulated in the roof zone had elevated K, Zr, Nb and Hf concentrations. The hydrothermal contribution significantly elevates the whole-rock concentrations of the HFSE in the LANS, but the LANS shows little evidence of REE enrichment. It is possible that the REE were preferentially concentrated into a Na-rich fluid that was subsequently expelled from the roof zone.

Late-stage hydrothermal processes: REE mineralised veins

The late-stage mineralised veins cross-cut the mafic lithologies at Jolotca and the country rock at Belcina (Hirtopanu et al., 2013b); historical mining, field, and mineralogical evidence indicate that these post-date crystallisation of the magmatic rocks, and were emplaced into a fracture system. The absolute age of the late mineralised veins is not known. The mineralised veins at both localities are characterised by multiple REE-bearing phases hosted in a carbonate gangue, and appear to be of hydrothermal origin as suggested by Hirtopanu et al., (2013). The available evidence indicates that the Belcina veins were likely formed by similar processes to those at Jolotca.

The mineralised veins have previously been the subject of exploration for REE, and their mineralogy clearly indicates high REE contents. The fluid that transported the REE in the mineralised veins was clearly carbonate-rich, and also contained ligands such as F- or Cl-, required to dissolve the REE (Williams-Jones et al., 2012). In the case of Ditrău, this fluid could either have been derived from the magmatic system, possibly by late-stage immiscibility within the magma chamber; or it could be derived from a separate source, possibly associated with late carbonatitic magmas. The presence of late-stage carbonate veins in the LANS, and the fact that REE preferentially partition into a carbonate-rich rather than silicate fluid (Mitchell, 2005) indicates that late-stage immiscibility is a possible explanation. A clue to resolving this comes from the apatite chemistry.

Small carbonate veins are present within the Ghiduţ nepheline syenite and LANS, and likely formed by late-stage exsolution of a carbonate-rich fluid in the magmatic-hydrothermal system. The carbonate vein apatites in the LANS (Ap_{CV}) have elevated concentrations of LREE, with a linear decreasing pattern, whereas the apatites from mineralised veins with a carbonate gangue have convex patterns with much higher concentrations of Y. Noticeably, Ap_{CV} do not have the same substitution mechanism as the apatite in the carbonate gangue of the mineralised veins (Ap_{MV}, Ap_{PY}, Ap_{ALN}; $REE^{3+} + SiO_4^{4-} = Ca^{2+} + PO_4^{3-}$ and $REE^{3+} + Na^{+} = 2Ca^{2+}$ respectively). This strongly indicates that the mineralised veins in the Jolotca area are derived from a distinctly different source to the fluids involved in alteration of the LANS, and provides convincing evidence for a potentially different source for the REE mineralised veins.

Hirtopanu et al., (2013a) suggest that the magmatic events at the Ditrău Complex concluded with a carbonatite melt which following the pathways of the previous alkaline melt, and was the source for the mineralising vein fluids. Late-stage carbonatites are certainly common in alkaline igneous complexes of this type, and there are at least two different phases of carbonate-rich fluid. Furthermore, the K-rich fluid that has caused alteration of mafic dykes and the LANS could be associated with the carbonatite magmatism, as is typical in fenites. It is thus clear that emplacement of a later carbonatite at depth, with release of both K-rich and carbonate-rich mineralising fluids into the complex, is a plausible explanation for the mineralisation at Ditrău. Further work would be needed to prove this hypothesis.

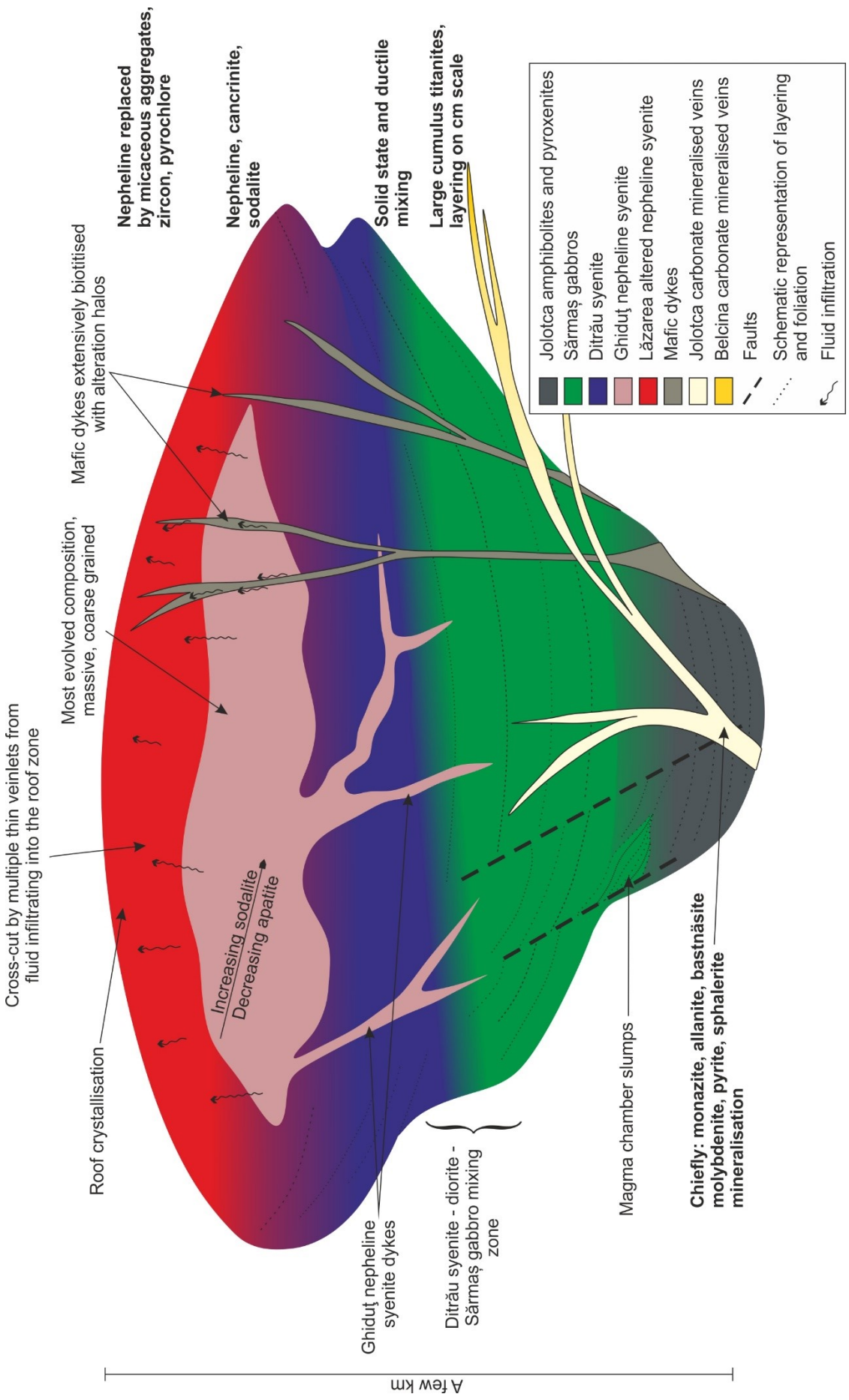

Figure 13. A schematic conceptual model produced for the Ditrău Complex. The complex is restored to horizontal.

CONCLUSIONS

The Ditrău Complex is an alkaline layered intrusion which was subsequently tilted during the Variscan orogeny. Fractional crystallisation in the magma chamber produced highly evolved nepheline syenites, but REE behaved compatibly at an early stage within the crystallising melt and are preferentially incorporated into titanite and apatite in ultramafic cumulates.

A hydrothermal system developed within the Ditrău Complex magma chamber during crystallisation, with patchy alteration of the nepheline syenites by a sodic fluid, and replacement of nepheline by cancrinite and sodalite. Subsequently, mafic dykes provided conduits for the uprise of late stage, potassic fluids which leached REE and HFSE from the syenitic rocks. These fluids reached the roof zone of the complex where they were trapped and percolated through the roof zone, causing the breakdown of nepheline to K-rich pseudomorphs and the deposition of hydrothermal minerals such as zircon and pyrochlore. However, the altered nepheline syenites of the roof zone do not show significant REE mineralisation.

The REE mineralisation at Ditrău is in mineralised carbonate-rich veins that cross-cut the complex and are known from the Jolotca and Belcina regions. From apatite mineral chemistry and petrologic study, they are clearly compositionally different to the other rocks of the complex, including those that are hydrothermally altered in the roof zone. The mineralised veins at both Jolotca and Belcina are considered here, to be related to the same late REE- and carbonate-rich fluid with pH controlled REE deposition. The source of that fluid may be a late-stage carbonatite emplaced into the alkaline igneous complex, but further work needs to be done to prove a carbonatitic source.

ACKNOWLEDGEMENTS

Many thanks to Strategic Resources Ltd for fieldwork assistance, particularly Radu Constantinescu, Mihai Cernaianu and Cristina Turea, and to Gyula Jakab for advice whilst completing this study's fieldwork. Thanks to Michael Stock and Victoria Smith at the University of Oxford and Chris Hayward from the University of Edinburgh for apatite EPMA advice, and Alicja Lacinska, Gren Turner and Jeremy Rushton at the British Geological Survey, Keyworth, for SEM help and advice. VCH acknowledges support from the Warwickshire Geological Conservation Group through their Holloway Award and the British Geological Survey for BUFI funding for an MSc project. VCH is supported by a Natural Environment Research Council studentship. KMG and RAS publish with the permission of the Executive Director of the British Geological Survey. This work is a contribution to the EURARE project, which is funded by the European Community's Seventh Framework Programme under grant agreement no. 309373.

REFERENCES

Anastasiu, N., Constantinescu, E., 1982. Tectonostructural position of the foidic rocks in the Romanian Carpathians. St Cerc Geol Geof Georg. Ser Geol Bucuresti 26, 33–45.

Anastasiu, N., Constantinescu, E., 1978. K-feldspars from the alkaline massif of Ditrău. Dări Seamă ale Şedinţelor, LXIV-1978, Mineral. 13–36.

Ayers, J.C., Zhang, L., Luo, Y., Peters, T.J., 2012. Zircon solubility in alkaline aqueous fluids at upper crustal conditions. Geochim. Cosmochim. Acta 96, 18–28. doi:10.1016/j.gca.2012.08.027

Balintoni, I., Balica, C., 2013. Carpathian peri-Gondwanan terranes in the East Carpathians (Romania): A testimony of an Ordovician, North-African orogeny. Gondwana Res. 23, 1053–1070. doi:10.1016/j.gr.2012.07.013

Balomenos, E., Davris, P., Deady, E., Yang, J., Panias, D., Friedrich, B., Binnemans, K., Seisenbaeva, G., Dittrich, C., Kalvig, P., Paspaliaris, I., 2017. The EURARE Project: Development of a Sustainable Exploitation Scheme for Europe's Rare Earth Ore Deposits. Johnson Matthey Technol. Rev. 61, 142–153. doi:10.1595/205651317X695172

Batki, A., 2009. Petrogenesis of Lamprophyres from the Ditrau Alkaline Massif. University of Szeged, Doctoral School of Geosciences.

Batki, A., Pál-Molnár, E., Dobosi, G., Skelton, A., 2014. Petrogenetic significance of ocellar camptonite dykes in the Ditrău Alkaline Massif, Romania. Lithos 200–201, 181–196. doi:10.1016/j.lithos.2014.04.022

Bernini, D., Audetat, A., Dolejs, D., Keppler, H., 2013. Zircon solubility in aqueous fluids at high temperatures and pressures. Geochim. Cosmochim. Acta 119, 178–187. doi:10.1016/j.gca.2013.10.054

Binnemans, K., Jones, P.T., Van Acker, K., Blanpain, B., Mishra, B., Apelian, D., 2013. Rare-earth economics: The balance problem. Jom 65, 846–848. doi:10.1007/s11837-013-0639-7

Blackburn, T.J., Olsen, P.E., Bowring, S. A, McLean, N.M., Kent, D. V, Puffer, J., McHone, G., Rasbury, E.T., Et-Touhami, M., 2013. Zircon U-Pb Geochronology Links the End-Triassic Extinction with the Central Atlantic Magmatic Province. Science (80). 340, 941–945. doi:10.1126/science.1234204

Brimhall, G.H., Agee, C., Stoffregen, R., 1985. The hydrothermal conversion of horndblende to biotite. Can. Mineral. 23, 369–379.

Codarcea, A., Codarcea-Dessila, M., Ianovici, V., 1957. Structure geologique du massif des roches alcalines de Ditrau. Rev Geol Geogr Acad Rom II 3–4, 385–515.

Dallmeyer, D.R., Kräutner, H., Neubauer, F., 1997. Middle-late triassic 40 Ar/39 Ar hornblende ages for early intrusions within the ditrau alkaline massif , Romania : implications for alpine rifting in the carpathian orogen. Geol. Carpathica 48, 347–352.

Deer, W.A., Howie, R.A., Zussman, J., 1992. An introduction to the Rock-Forming Minerals, Second. ed. Pearson Education Limited.

Dewey, J.F., Pitman, W., Ryan, W.B.F., Bonnin, J., 1973. Plate Tectonics and the Evolution of the Alpine System Plate Tectonics and the Evolution of the Alpine System. Geol. Soc. Am. Bull. 84, 3137–3180. doi:10.1130/0016-7606(1973)84<3137

Drake, M.J., Weill, D.F., 1975. Partition of Sr, Ba, Ca, Y, Eu2+, Eu3+, and other REE between plagioclase feldspar and magmatic liquid: an experimental study. Geochemica Cosmochim. Acta 39, 689–712.

Eby, G.N., Woolley, A.R., Din, V., Platt, G., 1998. Geochemistry and Petrogenesis of Nepheline Syenites:

Kasungu–Chipala, Ilomba, and Ulindi Nepheline Syenite Intrusions, North Nyasa Alkaline Province, Malawi. J. Petrol. 39, 1405–1424.

Edgar, A.D., 1964. Studies on cancrinites; Part 2, Stability fields and cell dimensions of calcium and potassium-rich cancrinites. Can. Mineral. 8, 53–67.

European Commission, 2017. Communication from the commission to the european parliament, the council, the european economic and social committee and the committee of the regions on the 2017 list of Critical Raw Materials for the EU URL: http://eur-lex.europa.eu/legal-content/EN/ALL/?uri=COM:2017:0490:FIN (accessed 9.28.17).

Fall, A., Bodnar, R.J., Szabó, C., Pál-Molnár, E., 2007. Fluid evolution in the nepheline syenites of the Ditrău Alkaline Massif, Transylvania, Romania. Lithos 95, 331–345. doi:10.1016/j.lithos.2006.08.005

Finch, A. a., 1991. Conversion of Nepheline to Sodalite During Subsolidus Processes in Alkaline Rocks. Mineral. Mag. 55, 459–463. doi:10.1180/minmag.1991.055.380.15

Fleet, M.E., Pan, Y., 1997. Rare earth elements in apatite: Uptake from H2O-bearing phosphate-fluoride melts and the role of volatile components. Geochim. Cosmochim. Acta 61, 4745–4760. doi:10.1016/S0016-7037(97)00292-5

Fleet, M.E., Pan, Y., 1995. Site preference of rare earth elements in fluorapatite. Am. Mineral. 80, 329–335.

Fujimaki, H., 1986. Partition coefficients of Hf, Zr, and REE between zircon, apatite, and liquid. Contrib. to Mineral. Petrol. 94, 42–45.

Geisler, T., Schleicher, H., 2000. Composition and U–Th–total Pb model ages of polygenetic zircons from the Vånga granite, south Sweden: An electron microprobe study. Geol Foren Stock. Forh 122, 227–235.

Geisler, T., Ulonska, M., Schleicher, H., Pidgeon, R.T., van Bronswijk, W., 2001. Leaching and differential recrystallization of metamict zircon under experimental hydrothermal conditions. Contrib. to Mineral. Petrol. 141, 53–65. doi:10.1007/s004100000202

Gill, R., 2010. Alkali rocks, in: Igneous Rocks and Processes: A Practical Guide. Blackwell Publishing, pp. 291–346.

Gillespie, M., Styles, M., 1999. BGS rock classification scheme. Classif. igneous rocks Volume 1.

Goodenough, K.M., Schilling, J., Jonsson, E., Kalvig, P., Charles, N., Tuduri, J., Deady, E. A., Sadeghi, M., Schiellerup, H., Müller, a., Bertrand, G., Arvanitidis, N., Eliopoulos, D.G., Shaw, R. a., Thrane, K., Keulen, N., 2016. Europe's rare earth element resource potential: An overview of REE metallogenetic provinces and their geodynamic setting. Ore Geol. Rev. 72, 838–856. doi:10.1016/j.oregeorev.2015.09.019

Graedel, T.E., Gunn, G., Espinoza, L.T., 2014. Metal resources, Use and Criticality in: Gunn, G. (Ed.), Criticals Metals Handbook. John Wiley & Sons.

Green, T.H., Pearson, N.J., 1987. An experimental study of Nb and Ta partitioning between T & rich minerals and silicate liquids at high pressure and temperature. Geochemica Cosmochim. Acta 51, 55–62.

Herbich, F., 1859. Die geologischen Verhältnisse des nordöstlichen Siebenbürgens, in: Jahrb Ungarn Geol Anstalt. pp. 293–350.

Hirtopanu, P., Andersen, C.J., Fairhurst, J.R., 2010. Nb, Ta, REE(Y), Ti, Zr, Th, U and Te rare element minerals within the Ditrau alkaline intrusive complex, Eastern Carpathians, Romania, in: Szakall, S., Kristaly, F. (Eds.), Mineralogy of Szekelyland, Eastern Transylvania, Romania. Csik County Nature and Conservation

Society, pp. 89–128.

Hirtopanu, P., Andersen, J.C., Fairhurst, R.J., Jakab, G., 2013a. Allanite-(Ce) and its associations, from the Ditrau Alkaline intrusive massif, east carpathians, Romania. Proc. Rom. Acad. 15, 59–74.

Hirtopanu, P., Fairhurst, R.J., Jakab, G., 2015. Niobian Rutile and its associations at Jolotca, Ditrau alkaline intrusive massif, East Carpathians, Romania. Proc. Rom. Acad. 17, 39–55.

Hirtopanu, P., Jakab, G., Andersen, C.J., Fairhurst, J.R., 2013b. Thorite, Thorogummite and Xenotime-(Y) occurrence in Ditrau Alkaline Intrusive massif, East Carpathians, Romania. Proc. Rom. Acad. 15, 111–131.

Hoeck, V., Ionescu, C., Balintoni, I., Koller, F., 2009. The Eastern Carpathians "ophiolites" (Romania): Remnants of a Triassic ocean. Lithos 108, 151–171. doi:10.1016/j.lithos.2008.08.001

Holtstam, D., Andersson, U.B., Broman, C., Mansfeld, J., 2014. Origin of REE mineralization in the B Bastnäs-type Fe-REE-(Cu-Mo-Bi-Au) deposits, Bergslagen, Sweden. Miner. Depos. 49, 933–966. doi:10.1007/s00126-014-0553-0

Hövelmann, J., Putnis, A., Geisler, T., Schmidt, B.C., Golla-Schindler, U., 2010. The replacement of plagioclase feldspars by albite: Observations from hydrothermal experiments. Contrib. to Mineral. Petrol. 159, 43–59. doi:10.1007/s00410-009-0415-4

Humphreys, D., 2014. The mining industry and the supply of critical minerals, in: Gunn, G. (Ed.), Critical Metals Handbook. American Geophysical Union and Wiley, pp. 20–40.

Ianovici, V., 1938. Considerations sur la consolidation du massif syenitique de Ditrau, en relation avec la tectonique de la region. CR Acad Sci Roum 2 689–694.

Jakab, G., 1998. Geologia Masivului alcalin de la Ditrău [Geology of Alkaline Massif from Ditrău – in Romanian]. Pallas-Akademia, Miercurea-Ciuc.

Krautner, H.G., Bindea, G., 1998. Timing of the Ditrau alkaline intrusive complex (Eastern Carpathians, Romania). Slovak Geol. Mag. 4, 213–221.

Kyle, P.R., Moore, J.A., Thirlwall, M.F., 1992. Petrologic Evolution of Anorthoclase Phonolite Lavas at Mount Erebus, Ross Island, Antarctica. J. Petrol. 33, 849–875.

Larsen, L.M., 1979. Distribution of REE and other trace elements between phenocrysts and peralkaline undersaturated magmas, exemplified by rocks from the Gardar igneous province, south Greenland. Lithos 12, 303–315. doi:10.1016/0024-4937(79)90022-7

Liferovich, R.P., Mitchell, R.H., 2006. Apatite-group minerals from nepheline syenite, Pilansberg alkaline complex, South Africa. Mineral. Mag. 70, 463–484.

Marks, M.A.W., Coulson, I.M., Schilling, J., Jacob, D.E., Schmitt, A.K., Markl, G., 2008. The effect of titanite and other HFSE-rich mineral (Ti-bearing andradite , zircon , eudialyte) fractionation on the geochemical evolution of silicate melts. Chem. Geol. 257, 153–172. doi:10.1016/j.chemgeo.2008.09.002

Matenco, L., Krézsek, C., Merten, S., Schmid, S., Cloetingh, S., Andriessen, P., 2010. Characteristics of collisional orogens with low topographic build-up: an example from the Carpathians. Terra Nov. 22, 155–165. doi:10.1111/j.1365-3121.2010.00931.x

McCreath, J. a., Finch, a. a., Simonsen, S.L., Donaldson, C.H., Armour-Brown, a., 2012. Independent ages of magmatic and hydrothermal activity in alkaline igneous rocks: The Motzfeldt Centre, Gardar Province, South Greenland. Contrib. to Mineral. Petrol. 163, 967–982. doi:10.1007/s00410-011-0709-1

McDonough, W.F., Sun, S., 1995. The composition of the Earth. Chem. Geol. 120, 223–253. doi:10.1126/science.243.4889.367

Mitchell, R.H., 2005. Carbonatites and carbonatites and carbonatites. Can. Mineral. 43, 2049–2068. doi:10.2113/gscanmin.43.6.2049

Miyashiro, A., 1974. Volcanic rock series in island arcs and active continental margins. Am. J. Sci. 274, 321–355.

Morogan, V., Upton, B.G.J., Fitton, J.G., 2000. The petrology of the Ditrau alkaline complex, Eastern Carpathians. Mineral. Petrol. 69, 227–265. doi:10.1007/s007100070023

Pál-Molnár, E., 2010. Rock-forming Minerals of the Ditrau Alkaline Massif, in: Szakall, S., Kristaly, F. (Eds.), Mineralogy of Szekelyland, Eastern Transylvania, Romania. Csik County Nature and Conservation Society, pp. 63–88.

Pál-Molnár, E., 2000. Hornblendites and diorites of the Ditró Syenite Massif. Dep. Mineral. Geochemistry Petrol. 172.

Pál-Molnár, E., Arva-Sos, E., 1995. K/Ar radiometric dating on rocks from the northern part of the Ditro syenite massif and its petrogenetic implications. Acta Mineral. Szeged 36, 101–116.

Pál-Molnár, E., Batki, A., Odri, A., Kiss, B., Almasi, E., 2015. Geochemical implications for the magma origin of granitic rocks from the Ditrău Alkaline Massif (Eastern Carpathians, Romania). Geol. Croat. 58, 51–66. doi:10.4154/GC.2015.04

Pan, Y., Fleet, M.E., 2002. Compositions of the Apatite-Group Minerals: Substitution Mechanisms and Controlling Factors. Rev. Mineral. Geochemistry 48, 13–49. doi:10.2138/rmg.2002.48.2

Pană, D., Balintoni, I., Heaman, L., 2000. Precise U-Pb zircon dating of the syenite phase from the Ditrau alkaline igneous complex. Stud. Univ. Babeş-Bolyai Geol. XLV 45, 79–90.

Parsons, I. a N., 1978. Feldspars and fluids in cooling plutons. Mineral. Mag. 42, 0–17.

Pearce, J.A., Cann, J.R., 1973. Tectonic setting of basic volcanic-rocks determined using trace-element analyses. Earth Planet. Sci. Lett. 19, 290–300.

Piccoli, P.., Candela, P.., 2002. Apatite in Igneous Systems. Rev. Mineral. Geochemistry 48, 255–292.

Popescu, G., 1985. Rb-Sr geochronological data on rocks of the Ditrau Massif. Arch. Geolex Harghita (Miercurea Ciuc).

Pyle, J.M., Spear, F.S., Wark, D. a., 2002. Electron Microprobe Analysis of REE in Apatite, Monazite and Xenotime: Protocols and Pitfalls. Rev. Mineral. Geochemistry 48, 337–362. doi:10.2138/rmg.2002.48.8

Rădulescu, D.., Peltz, S., Stanciu, C., 1973. Neogene Volcanism in the East Carpathians (Calimani-Gurghiu-Harghita Mts.), in: Symposium Volcanism and Metallogenesis. Geological Institute, Bucharest.

Reck, B.K., Graedel, T.E., 2012. Challenges in Metal Recycling. Science (80). 337, 690–695. doi:10.1126/science.1217501

Rimsaite, J., 1975. Natural Alteration of Mica and Reactions Between Released Ions in Mineral Deposits. Clays Clay Miner. 23, 247–255. doi:10.1346/CCMN.1975.0230312

Ronsbo, J.G., 1989. Coupled substitutions involving REEs and Na and Si in apatites in alkaline rocks from the Ilimaussaq intrusion, South Greenland, and the petrological implications. Am. Mineral. 74, 896–901.

Rønsbo, J.G., 2008. Apatite in the Ilímaussaq alkaline complex: Occurrence, zonation and compositional

variation. Lithos 106, 71–82. doi:10.1016/j.lithos.2008.06.006

Săbău, G., 2009. Ti-Nb-REE assemblages in the monazite veins at Jolotca , Ditrău alkaline Massif, in: Anastasiu N., Duliu O. (Eds.) Mineralogy and Geodiversity - Tributes to the Career of Professor Emil Constantinescu, Editura Academiei Române. Universităţii din Bucureşti, pp. 143–153.

Schmid, S.M., Bernoulli, D., Fügenschuh, B., Matenco, L., Schefer, S., Schuster, R., Tischler, M., Ustaszewski, K., 2008. The Alpine-Carpathian-Dinaridic orogenic system: Correlation and evolution of tectonic units. Swiss J. Geosci. 101, 139–183. doi:10.1007/s00015-008-1247-3

Schulze, R., Buchert, M., 2016. Estimates of global REE recycling potentials from NdFeB magnet material. Resour. Conserv. Recycl. 113, 12–27. doi:10.1016/j.resconrec.2016.05.004

Sharp, Z., Helffrich, G., 1989a. The stability of sodalite in the system NaAlSiO4-NaCl. Geochemica Cosmochim. Acta 53, 1943–1954.

Sharp, Z., Helffrich, G., 1989b. The stability of sodalite in the system NaAlSiO4-NaCl. Geochemica Cosmochim. Acta 53, 1943–1954.

Sheard, E.R., Williams-Jones, A.E., Heiligmann, M., Pederson, C., Trueman, D.L., 2012. Controls on the concentration of zirconium, niobium, and the rare earth elements in the Thor Lake rare metal deposit, Northwest Territories, Canada. Econ. Geol. 107, 81–104. doi:10.2113/econgeo.107.1.81

Silver, L.T., Deutsch, S., 1963. Uranium-lead isotopic variations in zircon: a case study. J. Geol. 71, 721–758.

Sinha, A.K., Wayne, D.M., Hewitt, D. a, 1992. The hydrothermal stability of zircon: Preliminary experimental and isotopic studies. Geochim. Cosmochim. Acta 56, 3551–3560. doi:10.1016/0016-7037(92)90398-3

Sirbescu, M., Jenkins, D.M., 1999. Experiments on the stability of cancrinite in the system Na2O-CaO-Al2O3-SiO2-CO2-H2O. Am. Mineral. 84, 1850–1860.

Sørensen, H., Larsen, L.M., 1987. Layering in the Ilimaussaq Alkaline Intrusion, South Greenland, in: Parsons, I. (Ed.), Origin of Igneous Layering. Springer Netherlands, pp. 1–28.

Speer, J.A., 1987. Evolution of magmatic AFM mineral assemblages in granitoid rocks: the hornblende + melt = biotite reaction in the Liberty Hill pluton, South Carolina. Am Miner. 72.

Stampfli, G.M., 2000. Tethyan oceans, in: Bozkurt, E., Winchester, J.A., Piper, J.D.A. (Eds.), Tectonics and Magmatism in Turkey and the Surrounding Area. Geological Society, London, Special Publications, pp. 1–23.

Stegen, K.S., 2015. Heavy rare earths, permanent magnets, and renewable energies: An imminent crisis. Energy Policy 79, 1–8. doi:10.1016/j.enpol.2014.12.015

Stock, M.J., Humphreys, M.C.S., Smith, V.C., Johnson, R.D., Pyle, D.M., EIMF, 2015. New constraints on electron-beam induced halogen migration in apatite. Am. Mineral. 100, 281–293.

Stormer, J.C., Pierson, M.L., Tacker, R.C., 1993. Variation of F and Cl X-ray intensity due to anisotropic diffusion in apatite during electron microprobe analysis. Am. Mineral. 78, 641–648.

Streckeisen, A., 1960. On the structure and origin of the Nepheline-Syenite Complex of the Ditroff (Transsylvania, Rumania), in: Rep 21th IGC Part 13. pp. 228–238.

Streckeisen, A., Hunziker, J.C., 1974. On the origin and age of the Nepheline Syenite Massif of Ditro (Transsylvania, Rumania). Schweiz Miner. Petr Mitt 54, 59–77.

Szakacs, A., Ioane, D., Seghedi, I., Rogobete, M., Pecskay, Z., 1997. Rates of migration of volcanic activity and

magma out put along the Calimani-Gurghiu-Harghita volcanic range, East Carpathians, Romania. Przegląd Geol. 45, 1106.

Tanaka, M., Oki, T., Koyama, K., Narita, H., Oishi, T., 2012. Recycling of rare earths from scrap, in: Handbook on the Physics and Chemistry of Rare Earths. pp. 159–212.

Thomas, J.B., Bodnar, R.J., Shumizu, N., Sinha, A.K., 2002. Determination of zircon/melt trace element partition coefficients from SIMS analysis of melt inclusions in zircon. Geochemica Cosmochim. Acta 66, 2887–2901.

Tiepolo, M., Oberti, R., Vannucci, R., 2002. Trace-element incorporation in titanite: constraints from experimentally determined solid/liquid partition coefficients. Chem. Geol. 191, 105–119.

U.S. Geological Survey, 2015. Mineral Commodity Summaries 2015: U.S. Geological Survey; Rare Earths.

Upton, B.G.J., Emeleus, C.H., Heaman, L.M., Goodenough, K.M., Finch, a. a., 2003. Magmatism of the mid-Proterozoic Gardar Province, South Greenland: Chronology, petrogenesis and geological setting. Lithos 68, 43–65. doi:10.1016/S0024-4937(03)00030-6

VanTongeren, J. a., Mathez, E. a., 2012. Large-scale liquid immiscibility at the top of the Bushveld Complex, South Africa. Geology 40, 491–494. doi:10.1130/G32980.1

Walters, A.S., Goodenough, K.M., Hughes, H.S.R., Roberts, N.M.W., Gunn, A.G., Rushton, J., Lacinska, A., 2013. Enrichment of Rare Earth Elements during magmatic and post- magmatic processes: a case study from the Loch Loyal Syenite Complex , northern Scotland. Contrib. to Mineral. Petrol. 166, 1177–1202. doi:10.1007/s00410-013-0916-z

Watson, E.B., Green, T.H., 1981. Apatite/liquid partition coefficients for the rare earth elements and strontium. Earth Planet. Sci. Lett. 56, 405–421. doi:10.1016/0012-821X(81)90144-8

Webster, J.D., Piccoli, P.M., 2015. Magmatic Apatite: A Powerful, Yet Deceptive, Mineral. Elements 11, 177–182. doi:10.2113/gselements.11.3.177

Whitney, D.L., Evans, B.W., 2010. Abbreviations for names of rock-forming minerals. Am. Mineral. 95, 185–187. doi:10.2138/am.2010.3371

Wilke, M., Schmidt, C., Dubrail, J., Appel, K., Borchert, M., Kvashnina, K., Manning, C.E., 2013. Corrigendum to Zircon solubility and zirconium complexation in H2O + Na2O + SiO2 +/- Al2O3 fluids at high pressure and temperature. Earth Planet. Sci. Lett. 373, 242–243. doi:10.1016/j.epsl.2013.04.010

Williams-Jones, A.E., Migdisov, A. a., Samson, I.M., 2012. Hydrothermal mobilisation of the rare earth elements-a tale of “ceria” and “yttria.” Elements 8, 355–360. doi:10.2113/gselements.8.5.355

Yang, W. Bin, Niu, H.C., Shan, Q., Sun, W.D., Zhang, H., Li, N.B., Jiang, Y.H., Yu, X.Y., 2014. Geochemistry of magmatic and hydrothermal zircon from the highly evolved Baerzhe alkaline granite: Implications for Zr-REE-Nb mineralization. Miner. Depos. 49, 451–470. doi:10.1007/s00126-013-0504-1

Zincenco, D., 1996. Rb-Sr contributions to the chronology of the Ditrau massif. Anal. Univ. Bucuresti.

Zlagnean, M., Tomus, N., Vasile, C., Vasile, I., 2000. Processing of valuable vein-minerals, as molybdenite, monzaite, magnetite, pyrite and ilmenite, in: Massacci, P. (Ed.), Proceedings of the XXI International Mineral Processing Congress. Elsevier, pp. 5–9.